Bombardment of HOPG with multiple charged ions

by

Lucas Vusi Ndala

Submitted in partial fulfilment of the requirements for the degree of

Magister Scientiae (Physics)

In the Faculty of Natural and Agricultural Sciences at University of Pretoria

Pretoria

August 2015

Supervisor/Promoter: Prof J. B. Malherbe

Co-supervisor: Dr E. E. Donets

Summary

Bombardment of HOPG with multiple charged ions

by

Lucas Vusi Ndala

Submitted in partial fulfillment of the requirements for the degree of (MSc) in Physics in the Faculty of Natural and Agricultural Science,University of Pretoria

Supervisor/Promoter: Prof. J. B. Malherbe
Co-supervisor: Dr E. E. Donets

Electron cyclotron resonance ion sources and electron string ion sources play an important role in the production of multi-charged ion beams. We have used these devices to irradiate highly oriented pyrolytic graphite with highly charged ions Kr^{27+} at a fluence of 4.2×10^{9} cm^{-2} and Ti^{5+} at a fluence of 1.6×10^{11} cm^{-2}. The two instruments were used to irradiate highly oriented pyrolytic graphite samples at Veksler and Baldin Laboratory of High Energies (VBLHE, JINR, Dubna) with the Krion-2 electron string ion source and electron cyclotron resonance ion sources at the Flerov Laboratory of Nuclear Reactions (FLNR, JINR, Dubna) irradiation facility.

We have designed the sample holder for electron string ion source and electron cyclotron resonance ion source. The sample holder was manufactured at University of Pretoria at the Department of Physics in South Africa. For this study I also assisted in the assembling of the vacuum chamber in Dubna, Russia and tested whether it had any vacuum leaks.

The basic principles and equations for the production HCI were reviewed together the design and operating principles of the electron string ion source and electron cyclotron resonance ion source. In a review of ion-solid interactions, special attention was given to the interaction of HCI with solid surfaces and the possible mechanisms operating during this type of interaction. The interaction of highly charged ions with solid surface depends on potential energy rather than kinetic energy. Because in all other ion-solid interactions kinetic energy transfer to the substrate dominates, the study of HCI interactions where the potential energy

of the ions are much larger than their kinetic energy becomes more interesting. Highly charged ions have a high amount of potential energy due to the ionization process. This high power deposition creates nano-structures on the surface such as craters and nano-hillocks on the nanometre scale and also provide a high amount of secondary ions and electrons.

The surface damage (or modifications) of highly oriented pyrolytic graphite after irradiated with Kr^{27+} and Ti^{5+} ions was investigated using the scanning tunnelling microscope in NanoScan Company, Moscow State University. The potential energy and kinetic energy of Kr^{27+} ions were 15.5 keV and 2.7 keV, respectively, while for the Ti^{5+} ions they were 0.185 keV and 50 keV. For Kr^{27+} ion bombarded sample the STM measurements showed protrusion (nano-dots) on the highly oriented pyrolytic graphite (HOPG) surface. For Ti^{5+} ions bombardment we could not identify with certainty any topographical changes on the highly oriented pyrolytic graphite (HOPG) surface. The STM results in this study were compared to similar studies by other groups. Other groups used different highly charge ions (HCI) with various charge states (and hence potential energy of highly charge ions) and different incident ion kinetic energies as compare to ours. Compared to our results and previous results, we found that there was a correlation between the average protrusion diameter and the potential energy of the bombarding highly charge ion and an agreement between our Kr^{27+} ion bombardment results and the published results.

UNIVERSITEIT VAN PRETORIA
UNIVERSITY OF PRETORIA
YUNIBESITHI YA PRETORIA

Declaration

I, Lucas Vusi Ndala, declare that the dissertation, which I hereby submit for the degree of MSc in Physics at the University of Pretoria, is my own work and has not been submitted by me for a degree at this or any other tertiary institution.

Signature: …….

Date: …….

Acknowledgements

I would like to acknowledge the following people for their support and valuable contribution in the success of my study.

- My academic promoters, Prof. J. B. Malherbe and Dr E. E. Donets for their guidance, support, discussion during the course of this study.
- The head of Ion Source, Prof. E. D. Donets for assistance with Electron String Ion Source.
- Prof. S. Bogomolov for assistance with Electron Cyclotron Resonance Ion Source.
- The NRF, for financial support that enabled my smooth study progress. .
- My darling wife, Kate, your love, respect, support and confidence in me, has made my journey so easy to accomplish.
- My family and friends, thank you for the love and support that you have given me.
- Above all, I thank the Lord my creator who has made it possible for me to walk and finish this journey with success.

TABLE OF CONTENTS

ABBREVIATIONS

A-Anode

AFM-Atomic force Microscope

AM-Analysing Magnet

AM-Axial Magnets

DB-Diagnostic Box

DT-Drift Tube

E-Electron Gun

ECRIS-Electron Cyclotron Resonance Ion Sources

ESIS-Electron String Ion Sources

EBIS-Electron Beam Ion Sources

EB-Extracting Box

EXT-Extract Ions

EXT-Extracting Electrode

FC-False Cathode

FLNR-Flerov Laboratory of Nuclear Reactions

FS-Focusing Solenoid

GI-Gas Inlet

HOPG-Highly Oriented Pyrolitic Graphite

HCI-Highly Charged Ions

JINR-Joint Institution of Nuclear Research

L1 and L2-Focus Lens

LINAC-Linear Accelerator

MI-Microwave Injection

NRF-National Research Foundation of South Africa

P-Plasma

QM-Quadrupole Magnet

RE-Reflector Electrons

RM-Radial Magnets

SPM-Scanning Probe Microscope

STM- Scanning Tunnelling Microscope

TB-Target Box.

UV-Ultraviolet

VBLHE-Verksler and Baldin Laborotary of High Energies

CHAPTER 1: INTRODUCTION

Multi-charged ion beam are mainly used for basic research in the field of accelerator physics. There are different kinds of instruments that are used to create multi-charged ions. In this study, the electron string ion source and electron cyclotron resonance ion source were used to produce multi-charged ion beam. These instruments play an important role in the creation of multi-charged ions for investigations of ion beam interactions with solid surface, which is the main goal of this study. The basic principles of these instruments are discussed in more detail in Chapters 2 and 3. Single charged or multi-charged ions can also be obtained by a number of different ion sources. To mention a few these sources include electron sources, negative ion sources, microwave ion sources, laser ion sources, high current gaseous ion sources, metal vapour vacuum arc ion sources, liquid metal ion sources and surface plasma cold cathode ion sources. The basic ideas behind these ion sources are briefly described below.

1.1 ELECTRON ION SOURCES

By allowing electrons to escape from a cathode material electron guns provide electrons for an electron beam in an electron ion source [www4]. However, an electron must be sufficiently energised to upscale it into a high energy state within the material and additional energy for it to escape the surface [Hil96]. The result will be an emission of electrons with a component of velocity perpendicular to the surface and kinetic energy at least equal to the work done in passing through the surface [Hil96]. The work function of a material is related to the total energy required to for it to give up electrons. The source is used in industrial materials processing, accelerators for lepton production, klystrons, and welding.

1.2 NEGATIVE ION SOURCES

Negative ion sources generate negative ions through the charge exchange method. There are two ways of performing this: (1) a proton beam with an energy of 10 keV travels through a negative biased foil and negative hydrogen beam is generated by electron capture. (2) The proton beam for gasses travels through a region which is filled with the gas. Sequential electron capture creates a negative hydrogen beam. Protons are changed to neutral H^0 and H^- and the gas is an electron donor. A few percent of the proton beam is changed into negative hydrogen ions. A maximum beam current of 200 μA can be obtained with these sources.

1.3 MICROWAVE ION SOURCES

In microwave ion sources, alternating electric fields (gigahertz (GHz) frequency range) are used to create a plasma without using electrodes [Fai13]. The energy of the microwave is coupled to the discharge through a waveguide. The plasma chamber is surrounded by direct current solenoids which can create an axial magnetic field. The solenoid's magnetic field also acts to confine the positive ions [Fai13]. Microwave ion sources are classified into two groups: electron cyclotron resonance ion sources and off-resonance microwave plasma. A description of electron cyclotron resonance ion sources is found in chapter 2.

1.4 LASER ION SOURCES

In laser ion sources, the source is used to vaporize and ionize a non-transparent target material. Laser ion sources create high current and high charge state beams of every element [Fai13]. A pulsed high power laser is directed towards the target through a potassium chloride salt window in the target chamber. During the laser beam bombardment with the solid, material is vaporized and ionized into a plasma. Inverse bremsstrahlung accelerates the electrons. The target atom is ionized to high charge state by the electron stepwise. The dense plasma quickly expands into a plasma long cloud which movies along the region of expansion until it reaches the extraction hole [Fai13]. The target chamber rests on a high volume platform to allow a beam to be extracted by a grounded electrode. Back streaming of electrons is prevented by a suppressor electrode.

The energy delivered by the laser ranges from 0.1 J to some tens of Joules per pulse [Fai13]. The power density on the target surface depends on the highest charge state. Power densities used are in the range of 10^{9} - 10^{16} W/cm^{2}. The expansion region length depends on the pulse length.

1.5 HIGH CURRENT ION SOURCES

In high current ion sources, ions are formed by electron impact ionization of a gaseous medium and creating a plasma [Bro89]. The plasma has a width of several centimetres and up to tens of centimetres. The electron density is 1×10^{13} cm^{-3}. The sources use magnetic fields

to restrict the plasma. The source is used in particle accelerators with ions for basic research, space propulsion, inertial confinement fusion, neutral injection to heat magnetically confined fusion plasma, materials treatment and ion implantation.

1.6 METAL VAPOUR VACUUM ARC ION SOURCES

The metal vapour vacuum arc ion sources use one of the following: either vaporization of the solid material or surface ionization, or metallic ion sputtering of the solid electrode by a plasma gaseous carrier. The plasma discharge in the middle of two metallic electrodes in vacuum is called the metal vapour vacuum arc. The ambient pressure is in the range of 10^{-4} - 10^{-6} mbar.

A beam can be extracted at a maximum voltage of 100 kV. The charge state distribution of the ions produced can contain multiply ionized species with a charge state up to about $q = 5+$ for some metals [Bro89]. The mean charge states are typically $\bar{q}$ = 2 to 3, therefore the mean energy of the beam ions produced can be 200 – 300 keV [Bro89]. The beam ions with a mean energy of 200 – 300 keV can be generated. The metal vapour vacuum arc ion sources are used in the large power electrical engineering.

1.7 LIQUID METAL ION SOURCES

In liquid metal ion sources, the source employs gallium (metal) which is heated to the liquid state. A strong electric field creates a Taylor cone. When the tip of the cone becomes sharper, the strong electric fields are produced up to a point when ions are formed by field evaporation [www3]. The source is employed in ion implantation and focused ion beam devices.

1.8 SURFACE PLASMA COLD CATHODE ION SOURCES

Since negative hydrogen ions are created on the cathode surface, these sources were called surface plasma sources. The negative hydrogen ions current where the first ion source was first significantly increased by adding caesium vapour was the magnetron (also called a

planotron). Belchenko and his team at the Budker Institute of Nuclear Physics carried out this work in the early 1970s [Bel74].

Vadim Dudnikov invented the H^- penning ion source [Dud75]. It was developed further at the same time as the magnetron source at the Budker Institute of Nuclear Physics in 1970s by Gennadii Dimov and Yuri Belchenko. According to Smith and his team [Smi94] a scaled up penning source was thus developed, which had the advantage of giving similarly (to a microwave ion source) high currents with low emittances.

1.9 MULTI-CHARGED IONS

Multi-charged ions are suitable for technological applications owing to the following fascinating properties: They have an enormous amount of potential energy because of the ionization process. When a single multi-charged ion bombards the solid surface, its potential energy stored results in local power deposition of 10^{12} – 10^{14} Wcm^{-2}. This high power deposition creates nano-structures on the surface, such as craters or nano-hillocks on the nanometre scale [Zsc09]. During the creation, linear accelerator and ring accelerators gain energy. For a linear accelerator, the energy gained is directly proportional to the ion charge state q. The energy gained by ring accelerators is scaled with q^2 (energy gained can be increased up to 3 orders of magnitude).

The study by Tona [Ton04] indicated that the interaction of highly charged ions with a solid surface captures an amount of electrons into the empty orbits of the ions. In this process, a large amount of potential energy is emitted within a short time of less than 100 fs in a small region of the surface. These interactions exhibit important characteristics as mentioned above. For example, Xe^{44+} can release over 100 electrons from a gold surface. During such interactions with the surface, the HCI captures a lot of electrons into the higher Rydberg orbitals and releases the electrons as a result of Auger decay processes. This is repeated several times until the highly charged ions become neutralised to form a hollow atom [Win99].

The work by TU Wien group [Aum11] observed with STM that hillock-like defects appeared on the original atomically flat surface after highly oriented pyrolytic graphite surfaces were irradiated with multiple charged Ar^{9+} ions. The number of these hillocks was in direct

correspondence with the ion fluence, which indicated that every single ion impact causes one protrusion. Surface reconstruction and characteristics of interstitial defects in HOPG was observed in the vicinity of most defects [Aum11].

1.10 APPLICATIONS OF MULTI-CHARGED IONS

Highly charged ions can be used in different fields [Zsc09]:

- In biotechnology, for the creation of pores in thin materials to support the insertion of membrane proteins;
- Ion sources for research in medicine and radiation biology;
- In material analysis, they can be used for analytical methods such as surface spectrometer, surface imaging, time-of-flight secondary ion mass spectrometry, and others;
- For the diagnostics of plasmas in fusion devices in the low energy range;
- Ion beam lithography;
- Nano-structuring of insulators and thin films;
- Potential sputtering;
- As a reference source for emission and absorption spectroscopy with ions of intermediate charge states in astrophysical experiments;
- Nano-structuring and high resolving metrology techniques and;
- Sources of electromagnetic radiation in the ultraviolet, extreme ultraviolet and visible light region for calibration purposes.

1.11 PROJECT OBJECTIVE

The aim of this study was to investigate the effect of irradiating highly oriented pyrolytic graphite (HOPG) with highly charged ions, viz. krypton ions (Kr^{27+}) and titanium ions (Ti^{5+}). The electron string ion source (Krion-2) was used for the krypton ions and the electron cyclotron resonance ion source was used for the titanium ions. The bombardment-induced topography on the samples was investigated by scanning tunneling microscopy (STM).

Special attention was given on reviewing the basic physical principle and equations for the production highly charged ions as well as the design and operating principles of the electron string ion source and electron cyclotron resonance ion source. In a review of ion-solid interactions, the interaction of highly charged ions with solid surfaces and the possible mechanisms operating during this type of interaction were discussed in some detail.

The specific experimental objectives of this project include:

- To design the sample holder for electron string ion source and electron cyclotron resonance ion source;
- To help assemble the vacuum chamber for the electron string ion source (Krion-2);
- To use scanning tunnelling microscopes in order to observe the morphology and topography of the highly oriented pyrolytic graphite before and after the two types of ion bombardments,
- To identify protrusions (nano-hillocks) or craters (holes) that subsequently appear on the HOPG after ion bombardment and measure its size.

1.12 HIGHLY ORIENTED PYROLYTIC GRAPHITE

Highly oriented pyrolytic graphite (HOPG) was used in this study, due to a few reasons. It is made of anisotropic materials with very interesting properties as is discussed below. Due to its lamella structure, clean and flat virgin surfaces are easily obtained. HOPG is easy to cleave, atomically flat and relatively inert, even in the air [Yin01]. It is fundamentally a two-dimensional material with strong covalent bonding in two-dimensional layers and weak van der Waals interactions between the layers [Yin01]. The atom within a single plane has three nearest neighbours [www1]. The sites of one sublattice upper layer (A) are at the centre of triangles defined by tree nearest neighbours of the other one lower layer (B). Highly oriented pyrolytic graphite has a layer with a honeycomb arrangement of carbon atoms. The nearest-neighbour distance and in-plane lattice constant a_0 are 1.42 Å and 2.46 Å. The layers are spaced apart 3.35 Å. The basal planes are stacked in the sequence of ABAB as shown in figure 1.1. The atomic arrangement of the HOPG crystal is illustrated below in figure 1.1.

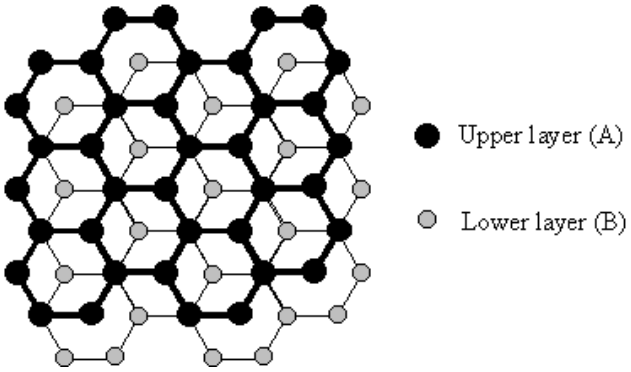

Figure 1.1: Highly oriented pyrolytic graphite crystal structure [www2].

The rest of the dissertation is organized as follows: Chapter 2 discusses production of multi-charged ions and provides a summary of its basic theory; chapter 3 elucidates the instrumentation used in this research; chapter 4 brings to view the interactions of ions with solid surfaces with special emphasis on highly charged ions; chapter 5 explains experimental procedures; chapter 6 presents the results and their discussion; and chapter 7 provides the final summary.

1.13 REFERENCES

[Aum11] F. Aumayr, S. Facsko, A. S. El-Said, C. Trautmann and M. Schleberger. "Single Ion Induced Surface Nanostructures: A Comparison between Slow Highly Charged and Swift Heavy Ions" Journal of Physics: Condensed Matter 23 (2011) 393001-23.

[Bac08] M. Bacal. "Physics Basis and Future Trends for Negative Ion Sources (invited)[a)]" Review of Scientific Instruments 79 (2008) 02A516-6.

[Bel74] Y. Belchenko, G. I. Dimov, and V. G. Dudnikov. "A Powerful Injector of Neutrals with a Surface Plasma Source of Negative Ions" Nuclear Fusion 14 (1974) 113-114.

[Bro89] I. G. Brown and R. Keller. "The Physics and Technology of Ion Sources" John Wiley & Sons 2 (1989) 137-417.

[Dud75] V.G. Dudnikov. "Proceedings of 4th AllUnion Conference on Charged ``Particle Accelerator" Moscow 1 (1974) 323-325.

[Fai10] D. S. Faircloth, S. R. Lawrie, A. P. Letchford, C. Gabor, M. Whitehead, T. Wood, and M. Perkins. "Latest Results from the Front End Test Stand High Performance H^- Ion Source at RAL" Proceedings of NIBS2010 Takayama Japan MOPD 057 (2010) 813-815.

[Fai13] D. Faircloth. "Ion Sources for High Power Hadron Accelerators" arXiv preprint arXiv:1302.3745 (2013) 369-407.

[Hil96] C. E. Hill. "Ion and Electron Sources" Cern European Organization for Nuclear Research Reports Cern (1996) 95-111.

[Kel10] R. Keller. "High Intensity Ion Sources for Accelerators with Emphasis on H^- Beam Formation and Transport (invited) a)" Review of Scientific Instruments 81 (2010) 02B311-8.

[Nik95] S. Nikiforov, V. Golubev, D. Solnyshkov, M. Svinin, and G. Voronin. "Ion Sources for use in Research and Applied High Voltage Accelerators" Proceedings of the PAC 95 (1995) 1004-1006.

[Pas89] F. Paschen and E. Wiedemann. "On the Radio Required for the Transition ... Potential Difference" Annual Review of Physical Chemistry 37 (1889) 69-96.

[Pie93] H. O. Pierson. "Handbook of Carbon, Graphite, Diamond and Fullerenes: Properties, Processing and Applications" William Andrew Publishing/Noyes,New York (1993).

[Scr04] Scrivens, R. "Proton and Ion Sources for High Intensity Accelerators" No. CERN-AB 075 (2004) 1-6.

[Smi94] H. V. Smith, P. Allison, and J. D. Sherman. "H^- and D^- Scaling Laws for Penning Surface Plasma Sources" Review of Scientific Instruments 65 (1994) 123-128.

[Ton04] M. Tona and S. Takahashi. "Highly Charged Ion Beams from the Tokyo EBIT for Applications to Nano-Science and Technology" Journal of Physics: Conference Series. IOP Publishing 2 (2004) 57-64.

[Uen04] A. Ueno, K. Ikegami, and Y. Kondo. "Surface Production Dominating Cs^- free H^- Ion Source for High Intensity and High Energy Proton Accelerators" Review of Scientific Instruments 75 (2004) 1714-1719.

[Win99] H. Winter, and F Aumayr. "Hollow Atoms" Journal of Physics B: Atomic, Molecular and Optical Physics 32 (1999) R39-R65.

[www1] www.nanoprobes.aist-nt.com, 3rdJanuary 2014.

[www2] www.spmtips.com, 19th February 2014.

[www3] www.en.wikipedia.org/wiki/Ion_source, 4th March 2014.

[www4] www.nau.edu/microanalysis/microprobe-sem/instrumentation.htm1, 5th March 2014.

[Yin01] Z. Yingjie, J. D. McBride, T. A. Hansen, and T. P. Beebe. "Controlled Production of Molecule Corrals using Cesium Ion Bombardment: a TOF-SIMS, XPS, and STM Study" The Journal of Physical Chemistry B 105 (2001) 2010-2018.

[Zsc09] G. Zschornack, F. Grossmann, V. P. Ovsyannikov, R. Heller, U. Kentsch, M. Kreller, M. Schmidt, A. Schwan, A. Silze, and F. Ullmann. "Sources of Highly Charged Ions as a platform Technology for Applications in Nanotechnology and Medicine" Materialwissenschaft und Werkstofftechnik 40 (2009) 285-289.

CHAPTER 2: PRODUCTION OF MULTICHARGED IONS

Multi-charged ions can be produced by different ion sources, some of which were described in Chapter 1. However, the production of highly charged ions with a charged state of $q^+ > 10$ is possible with only three kinds of ion sources:

- Electron Beam Ion Source (EBIS),
- Its modification, the Electron String Ion Source (ESIS), and
- Electron Cyclotron Resonance Ion Source (ECR).

In this project we shall discuss in detail the production of highly charged ions (HCI) by these three ion sources. We shall start with electron impact ionization principles, which are the background of HCI production. The physics and technical aspects of EBIS, ESIS and ECR ion sources shall then be described in detail.

2.1 ELECTRON IMPACT IONIZATION

Electron impact ionization is a physical process that is used in an electron beam ion source to produce highly charged ions. The electron impact ionization is the main process leading to high ion charged states. Multiple electron-ion collisions are needed in order to sequentially remove one electron from an electron shell of the ion resulting from a single collision.

The main characteristic entity describing an EBIS/ESIS is the ionization factor, i.e., the product $j_e\tau/e$, where the electron beam current density j_e [Ampere/cm^2] is in the direction orthogonal to the electron beam propagation, and ionization time τ [s] is time needed to reach definite charge state Q^{k+} and e is the electron charge. The electron beam energy should exceed the binding energy E_{-k} of the *k-th* electron of the given atom, starting from an outer electron.

The basic equation describing the probability of transition of an ion from charge state q to charged state $(q+1)$ is given as:

$$P_{q\to q+1} = \sigma_{q\to q+1} j_e \tau/e \qquad (2.1)$$

where $\sigma_{q\to q+1}$ is the effective cross section ionization of ion, with a charge state q by electron collision. Therefore, on average, all charge state ions q change to the charge state $(q+1)$ when $j_e\tau = \frac{e}{\sigma_{q\to q+1}}$. This means that to produce ions of mean charge k from single charged ions with stepwise ionization, the ionization factor has to be:

$$j_e\tau = \sum_{q=1}^{k-1} e/\sigma_{q\to q+1}^{-1} \qquad (2.2)$$

The first semi-empirical formula to calculate direct ionization cross-sections was introduced by Tompson in 1912 [Lot67] with the following equation:

$$\sigma_k = \frac{\pi n a_0^2}{I_k E_e}\left(1 - \frac{I_k}{E_e}\right) \qquad (2.3)$$

where I_k , E_e and n represent the *k-th* ionization electron energy, the electron beam energy given in atomic units (one atomic unit is equal to 13.6 eV) and the number of electrons in the outermost subshell. The a_0 is called the Bohr radius (a_0 = 0.529 x 10^{-10} m).

In practice, the effective cross sections $\sigma_{q\to q+1}$ for the ionization of an ion with an arbitrary charge state q can be estimated using Lotz's semi-empirical formula below [Lot67]:

$$\sigma_{q\to q+1} = \frac{4.5\times10^{-14}}{E_e}\sum_{n=n_q}^{n_{min}} \frac{k_{nl}}{I_{nl}} ln\frac{E_e}{I_{nl}} \quad (\text{cm}^2) \qquad (2.4)$$

where E_e denotes electron impact beam energy, I_{nl} is the binding energy for electron i in subshell nl, the energy is given in eV and the sum is overall removable electrons in all orbits nl, n is a main atomic quantum number, n_q is the main quantum number of an outer shell for a given ion with charge state q, I_{nl} is the ionization potential of the nl-subshell for the given ion with charge state q, k_{nl} is the equivalent electrons number of nl-subshell for the given ion q and n_{min} is the minimal value of n, for which the ratio $\frac{E_e}{I_{nl}} > 1$.

Thus, substituting equation (2.4) into (2.2) the ionization factor required to obtain any ion charge state can be estimated.

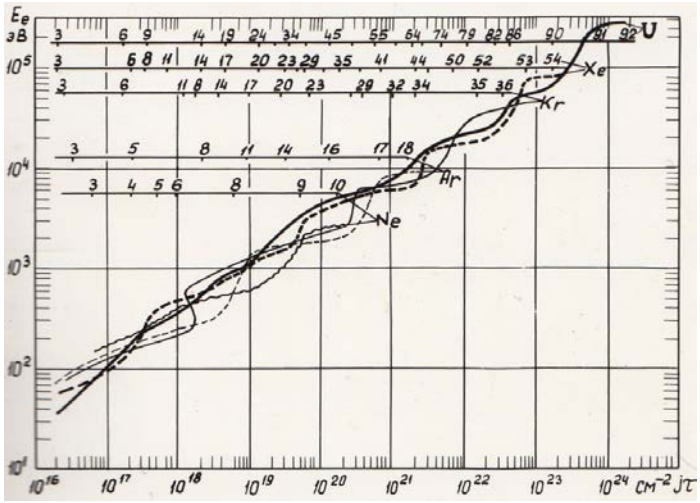

Figure 2.1: The ionization factor values required to create charge states of Ne, Ar, Kr, Xe and U ions [Don77].

The determined values of the ionization factor $\frac{j_e}{e}\tau$ required to acquire Ne, Ar, Kr, Xe and U ions of all charges are given in figure 2.1. One can see from this figure 2.1, that, for example, in order to produce a Kr bare nuclei (Kr^{36+}), one needs to have an electron beam energy about 30 keV, and the ionization factor has to be about $\frac{j_e}{e}\tau = 3 \times 10^{22}$ [1/cm^2]. Thus, if the electron beam current density is about $j_e \approx 1000$ [A/ cm^2], bare Kr^{36+} ions can be produced, starting with neutral Krypton atoms, for the ionization time $\tau \approx 4.8$ s; (note, $e = 1.6 \times 10^{-19}$ C).

In this dissertation, we shall describe experiments with an ion beam of Kr^{27+}, produced by Krion-2 ESIS (JINR, Dubna). Thus, following the same lines, we shall get the necessary ionization factor $\frac{j_e}{e}\tau = 2 \times 10^{20}$ [1/cm^2] with the electron beam energy of about 5 keV. The electron current density of the Krion-2 ESIS was about $j_e \approx 250$ [A/ cm^2], that gives the ionization time to reach Kr^{27+} to be equal to $\tau \approx 0.13$ s.

2.2 ELECTRON BEAM ION SOURCE (EBIS)

The EBIS concept was first proposed and realized in JINR, Dubna in 1967 [Bro89], and from the beginning of its development the main goal was the creation of conditions for the production of extremely highly charged ions, including bare nuclei of heavy elements.

The electron beam ion source is a device for the production of multiply charged ions in a pulse mode of operation that involving:

- The production of an extended electron beam of given energy and density;
- The creation of an electrostatic ion trap along the beam;
- The injection of a definite number of low charge state ions (or neutral atoms) of the working substance into the trap during a definite period of time;
- Containment of the ions in the electron beam for a period of time sufficient for the ions to reach the desired charge state;
- Extraction of these highly charged ions from the trap along the electron beam and preparation for the next cycle.

Simply stated, the EBIS concept is realized in the following way: the EBIS, illustrated in figure two, uses a dense mono-energetic electron beam, produced by the electron gun. The electron gun is arranged at the fringe magnetic field created by a surrounding solenoid. The

emitted electron beam is further focused and compressed by the strong magnetic field in the ionization trap region, which is in a uniform maximal magnetic field (up to few Tesla) inside the solenoid.

Neutrals, which become singly charged ions immediately when subjected to a dense electron beam, injected into the EBIS are limited radially by the electrostatic forces from the negatively charged electron beam and magnetic field from the solenoid. It is also confined longitudinally by the potential barriers produced by cylindrical electrodes surrounding the beam [Bro89]. Inside the trapping region the high energy electrons collide with ions, which are ionised stepwise, until they are extracted by raising the trapping potential and lowering the extraction barrier simultaneously.

Inside the trap, the ions oscillate radially in the electrostatic field of the beam with a superimposed azimuthal cyclotron motion around magnetic field lines with bouncing between end barriers which is not complementary [Bro89]. A schematic diagram of an electron beam ion source is represented below in figure 2.2:

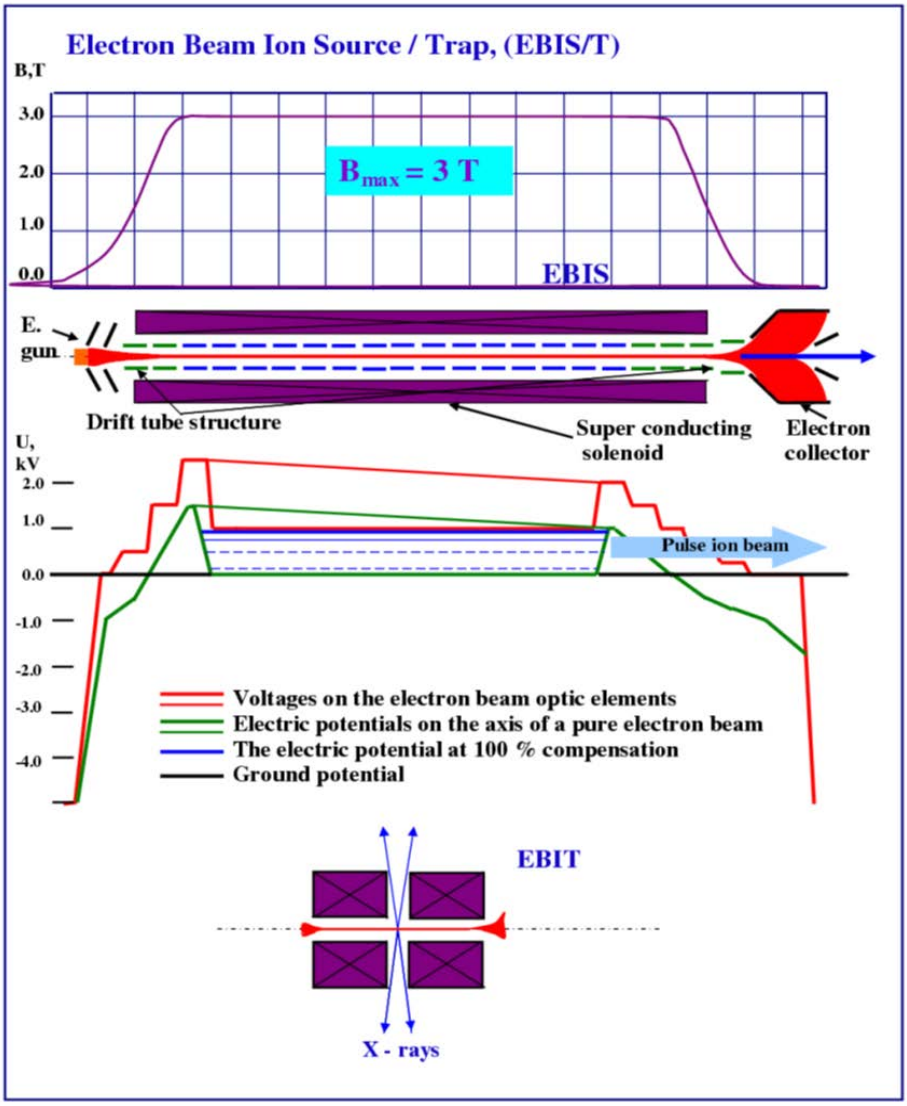

Figure 2.2: A schematic diagram of the electron beam ion source (EBIS) Krion-2, JINR, Dubna, top; and the electron beam ion trap (EBIT), bottom.

Now we consider all these aspects in more detail.

2.2.1 PRODUCING AN EXTENDED ELECTRON BEAM OF GIVEN ENERGY AND DENSITY

In order to obtain a dense extended electron beam, it is necessary to ensure that the beam has a constant shape and cross section over the drift length. A longitudinal magnetic field is

usually applied for this. There are three main modes of electron beam formation, which provide sufficiently different values of the beam density for a given magnetic field induction (B) in the drift space: The first mode involves magnetic ducting: where j_e is constant and is limited by the emissivity of the cathode of the gun; the second is by using magnetic compression: where j_e is proportional to B ; and through Brillouin focusing: in which case j_e is proportional to B^2.

A modern EBIS operates with a magnetic compression method. In this case an electron emitter is placed in a fringe magnetic field of a main solenoid in a position where $B_c \approx B / n$, where B is a magnetic induction at the central region of solenoid, n is a number which can vary in a wide range, i.e. n = (2 - ∞). The electron beam, being emitted by an electron emitter, penetrates into a drift tube space at the central part of the solenoid following the magnetic flux lines and, thus, its radial size shrinks $\sqrt{n}$ times, providing a corresponding magnetic compression $j_e \propto n\ B$. However, this simple estimation holds for moderate values of $n < 100$ only.

In a general case, the thermionic properties of the emitted electrons should be taken into account. Indeed, a zero temperature electron gas accurately initiated from a cathode located at zero magnetic fields ($n = \infty$) would be anticipated to be compressed by a magnetic field to form a beam with a characteristic radius equivalent to the Brillouin radius expressed as:

$$r_b = \frac{150}{B[T]}\sqrt{\frac{I_e[A]}{\sqrt{E_e[keV]}}} \qquad (2.4)$$

where I_e and E_e are the electron beam current and the electron beam energy respectively at the trap with the dimensions of the quantities being given in square brackets. The electron emission (thermionic) is due to a nonzero temperature, and then equation (2.4) can give an excessively high estimate squeezing attained. This condition allows the theory of Herrmann [Her58] to provide a fine estimation of determining the radius where 80 % of the beam passes as:

$$r_h = r_b\sqrt{\frac{1}{2}+\frac{1}{2}\sqrt{1+4\left(\frac{8kT_c r_c^2 m}{e^2 r_b^4 B^2}+\frac{B_c^2 r_c^4}{B^2 r_b^4}\right)}} \qquad (2.5)$$

Here, r_c and kT_c represent cathode radius and characteristic electron energy at the cathode, m is the mass of the electron, e is the charge of the electron, B_c and $B = B_{max}$ are the magnetic field at the cathode, and the maximum magnetic field in the trap region.

The beam radius becomes a minimum when B_c is less than or equal to zero. As a result, an electron beam ion source is shielded with soft iron and coil bucking inclusion to the major solenoid. In reality, the best performance of the extracted ions produced is due to the coil bucking the current. Provided the ratios in round brackets are dimensionless, any system of units can be used for the quantities in equation (2.5), with r_h and r_b having the same units of micrometres. The parameter r_b is taken from equation (2.4), the first term in round brackets is generally much greater than unity. Due to comparatively small constants, applying $B_c = 0$ and changing to appropriate units, the smallest achievable radius beam can be given as:

$$r_h = \left(\frac{8mkT_c}{e^2}\right)^{1/4} \sqrt{\frac{r_c}{B}} \approx 2.59 \times 10^{-3} T_c^{1/4} \sqrt{\frac{r_c}{B}} \qquad (2.6)$$

with T_c in electron-volts and all other quantities in SI-units. Thus, one gets maximum current density achievable with the use of a magnetic compression method.

$$j_e = \frac{I_e}{\pi r_h^2} \propto \frac{1.49 \times 10^5}{r_c T_c^{1/2}} B \qquad (2.7)$$

Electron beam energy is steered by the emitter-anode voltage in an electron gun. The emitter-anode distance in an electron gun usually takes a few mm; the anode has an orifice in its prexial part for electron propagation towards a drift tube structure at the central part of solenoid. After one pass through drift tube structure, the electron beam is collected on a special electron collector, which is arranged at the opposite end of the EBIS in a weak enough magnetic field. An electron collector is placed off-axially, thus electrons are bent from magnetic axis electrostatically to reach a collector; in a contrast to this, the produced ions are extracted from the EBIS along the magnetic axis providing a minimal emittance growth of the ion beam due to its extraction from the solenoidal magnetic field.

2.2.2 CREATING AN ELECTROSTATIC ION TRAP ALONG THE BEAM

We consider the electric potential of the space charge of the cylindrical electron beam passing inside a drift tube with a definite potential. In the ideal case of an axial symmetry (i.e., the beam axis coincides with the geometrical axis of the surrounding cylindrical tube) it is known [Bro89] that the radial electric potential distribution has the form:

$$U(r) = U_{dr} + 2s^{-}ln\frac{R}{r} \qquad (r > r_0) \qquad (2.8)$$

$$U(r) = U_{dt} + s^{-}\left[2ln\frac{R}{r_0} + \left(1 - \frac{r^2}{r_0^2}\right)\right] \qquad (r < r_0) \qquad (2.9)$$

where U_{dt} and s^{-} are the potential of the drift tube and the linear charge density of the electrons of the beam, whereas R is the internal radius of the drift tube, r_0 is the radius of the beam, and r is the cylindrical coordinate.

A simple estimate shows that in the axially symmetric case equation (2.9), the depression in the potential *U(r),* produced by the space charge of an electron beam of 10 keV energy and

1 A current, is equal to about 150 eV. Such a depression can be used for radial ion containment in the electron beam. To vary the potential along the axis of the system, the simplest way is to make a drift tube in separated sections and apply different potentials to different sections.

If in an ion-free electron beam system a low energy ion of charge state q^{+} is created at a point $r < R$, it cannot reach the wall of the *(R)* without gaining energy; the potential depression of the beam space charge provides radial trapping of the ion. To close the electrostatic trap in the axial direction, it is sufficient to apply a potential

$U_t \geq \left|s^{-}\left[2ln\frac{R}{r_0} + 1\right]\right|$ at the end sections of the system. If an electron beam is filled with ions, the positive charge of the ion partially compensates the potential depression of the electron beam space charge. In this case, the value of the electrostatic potential which the closes the electrostatic trap in an axial direction should be increased correspondingly.

2.2.3 INJECTING A DEFINITE NUMBER OF LOW CHARGE STATE IONS (OR NEUTRAL ATOMS) OF THE WORKING SUBSTANCE INTO THE TRAP IN A DEFINED PERIOD OF TIME

The most uncomplicated method of filling the trap with ions is to generate them directly in the trap from the atoms of a cloud of the working substance by electron impact in the electron beam. In this method of injection, ions are born in the trap with a very small kinetic energy compared to $-q_i s^{-}$ (s^{-} is a linear charge density of the electron beam), which is a maximum potential energy of a newly born beam ion of charge state q_i. One can consider ion motion within the trap in the single-ion model. When the electron beam passes through the cloud of the working substance, mostly singly charged ions are produced with equal probability at any

point r_i. The ions then execute oscillatory motion about the point of minimum potential. In the axisymmetric case and without magnetic field, the ion radial motion can be described by the expression:

$$r = r_i cos\left(\frac{q_i|\rho|}{2M\varepsilon_0}\right)^{1/2} \quad t \equiv r_i cos(w_i t); \tag{2.10}$$

where ρ is a volume density of the negative charge of the electron beam, q_i is a charge state of the ion, M is the ion mass, ε_0 is the dielectric constant and the ion plasma frequency w_i is introduced. If a magnetic field is applied, the equation of radial motion (2.10) will be more complicated. However, one can describe the ion behaviour qualitatively. For example, the trajectory of single charged O^{1+} ion for B = 2 Tesla, ρ = 3.2 x 10^{-8} C / cm^3 (2 x 10^{11} electronic charges / cm^3), r_i = 0.15 cm moves at the point r = 0 with frequency of 1.05 x 10^8 rad/s. This example corresponds to the real case of a beam current I_e = 0.13 A, current density 200 A / cm^2 and 10 keV electron energy.

Thus, in the single-ion model, there is a range of ion energies that lie between 0 and $-q_i s^-$ with a constant number of ions per unit energy range. In their motion, they do not leave the beam. This is requisite for further ionization. But in this case, the number of ions in the beam is relatively small; single-ion model is valid if the compensation level of an electron beam space charge by positively charged ions is small, i.e., $S^+ \leq 10^{-2}\,|S^-|$, where S^- is a linear charge density of the electron beam.

The method of pulse injection of ions into an electron beam is used in practise to inject more ions into the electron beam. In principle, one can use a pulse generated cloud of atoms of the working gas and regulate the number of the injected atoms in each pulse in order to avoid overcompensation in the injection region of the ion trap $S^+ \approx |S^-|$. But almost always it is technically a very difficult operation. Alternatively, the working gas enters the injection region continuously and the electron beam intercepts the gas cloud in this region, with an appropriate axial potential distribution to ensure that the actual position of interception is within the electrostatic trap for only a controlled interval of time.

2.2.4 CONTAINMENT OF THE IONS AND IONIZATION

The initial charge state q_{in} of ions injected into the trap are contained in the electron beam for the ionization time τ_i in order to reach the mean final charge state q_f. The ionization time is given by:

$$\tau_i = \frac{1}{j_e} \sum_{q_{in}}^{q_f - 1} e\sigma_{q \to q+1}^{-1} \qquad (2.11)$$

In the single-ion model, the motion of ions during ionization is assumed in (2.10). Ions can be ionized at any point of their trajectory inside the electron beam. However, the greatest probability of ionization is near the equilibrium positions, where the potential energy is maximum and the ion velocity is approximately zero. If q increases at the point of production of the ion at r_{imax} , then in the absence of a magnetic field the trajectory does not change. However, the energy E_1 of the ion increases in proportion to q, $\omega_i \sim q$ and r_{imax} are conserved since the rigidity changes non-adiabatically. Similar changes take place in the presence of the magnetic field. But if q increases at $r_i < r_{imax}$, the ion cannot subsequently reach $r_i = r_{imax}$, although E_i and ω_i increase. At the end of the ionization process, the energy spread of the ensemble ions was increased $(E_i - q_i s^- \geq 0)$, with an increase in energy, where ω_i increased with q with increased in frequency and decreased with values of r_i, that could result in more or less significant concentration of ions in the direction of the beam axis. There are three modes in the self consistent field model that have to be taken into consideration.

- Following injection, the electron beam is filled with slow ions, resulting in $S^+ \approx |S^-|$. Due to multiple ionization S^+ becomes greater than $|S^-|$ and a force due to a radial loss appear for ions. Ions move out to the drift tube wall, with a delay because of their motion across the magnetic field. This leads to some disadvantages. Since the more highly charged ions have a greater velocity, they leave the beam more rapidly and after recombination on a drift tube wall some of them can return onto the beam. In this case one has a non-conserved number of ions in the trap, which renders analysis more complicated.
- A core of ions with near-thermal energies is formed as a result of injection into the axial region of the beam so that, in this region, the charge of the beam is fully compensated while the main part of the beam is free of ions. The region with ions will be overcompensated by the ion charge during the ionization process. Also, if at the beginning of the ionization the containment voltage at the end sections of the trap is increased, then the ions cannot leave the trap in the axial direction. The result is that their charge compensates the region of the beam that is free of ions. In this case it is possible to obtain the maximum number of ions of the final charge state, since at the end $S^+ = |S^-|$.

- In the simplest case considered above, ions are moving during their containment time in the field of the electrons or of an ion-electron space charge. However, there are various sources of ions heating that can change the ion motion, which lead to thermal losses of ions from the beam. In particular, the heating of ions by Coulomb collisions with the beam electrons is a main source of ion thermal losses. Well-known two-stream instability is also a source corresponding to ion losses from the beam. All these factors should be taken into account.

2.2.5 CHARGE STATE EVOLUTION

Ionization processes in an electron beam and the corresponding charge state evolution are of particular interest. The evolution can be described in a form of solutions of a system of ordinary differential equations with a real time (t) evolution parameter.

For ion species with charge state q, we define N_q as the total number of such ions in the trap, where N_q^{in} represents the number of such ions inside the electron beam. It therefore becomes possible to define $f_{e,q} \equiv \frac{N_q^{in}}{N_q}$ as a ratio of ions inside the electron beam to ions in the trap.

Charge transfer and double ionization have cross sections at least an order of magnitude less than their single counterparts in general and so these two processes can be neglected. Charge exchange happens through ion–neutral collisions when the trapped ion temperature is sufficiently low. The Coulomb barrier prevents ion-pairs coming close enough for charge exchange to occur. This is a simplified model since adjacent charge states are only coupled to each other. In reality, ions can also escape from the trap in the manner described above. However, a series of coupled differential equations, one for each charge state can describe these processes in a general case:

$$\frac{dN_q}{dt} = \frac{j_e}{e}\left(N_{q-1}\sigma_{q-1}^{EI} f_{e,q-1} - N_q\sigma_q^{EI} f_{e,q}\right) + \frac{j_e}{e}\left(N_{q+1}\sigma_{q+1}^{RR} f_{e,q+1} - N_q\sigma_q^{RR} f_{e,q}\right) + \mathcal{E} + i \quad (2.12)$$

The first equation of (2.12) describes electron impact ionization (EI). There are two terms in brackets, accounting for the creation of species (charge state) q from species *q-1* (hence, positive sign) and for annihilation of species q along with creation of species *q-1* (hence, negative sign). Similarly, the second equation of (2.12) describes creation and annihilation of species q by radiative recombination (RR), where $\mathcal{E}$ is the charge exchange and i represents

the ion losses. Radiative recombination is a process opposite to electron impact: it is a capture of the beam electrons by the ions. Electron-impact ionization and the radiative recombination process occur during the electron interactions from the electron beam. Thus, the cross sections are functions of the electron beam energy and the associated rates relate linearly with the current density j_e.

The electron impact ionization cross section σ^{EI} increases from zero at the threshold (equal to the binding energy of the given charge state) to peak at two or three times the ionization potential associated with the reaction. This peak may occur at high energy for highly charged states. As more electrons are removed from the target the electron impact ionization cross section becomes smaller, i.e., it becomes smaller for increasing q. However, the radiative recombination cross section σ^{RR} is approximately $\frac{q^4}{\sqrt{E_e}}$.

The third term should describe charge exchange between ions and other light ions or neutrals, which can penetrate in the ion trap even if vacuum conditions are about 1.33×10^{-12} mbar. The last term should describe thermal ion losses from the trap caused by ion heating, described briefly above. One can neglect two last effects and consider charge state evolution taking into account electron impact ionization and radiative recombination only.

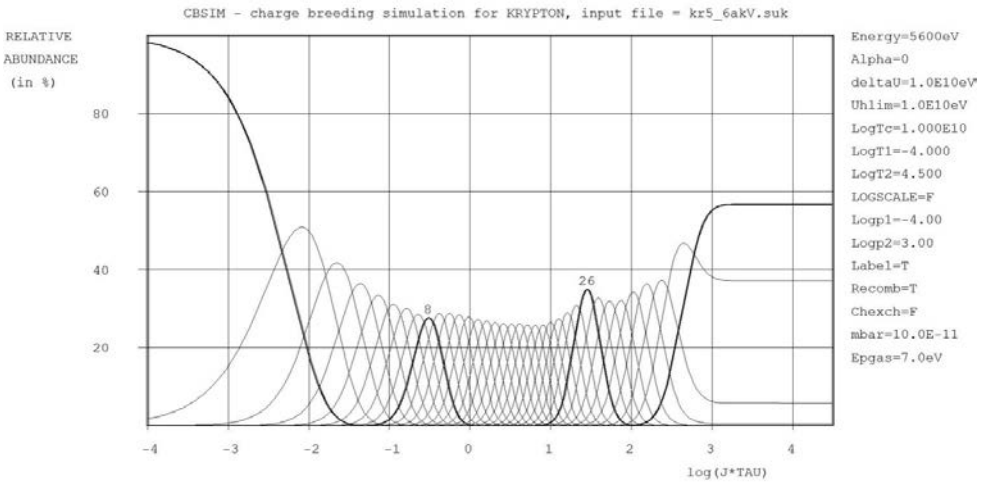

Figure 2.3: Relative abundances (in percentages) of charge state species of krypton versus log $(j_e\tau)$ (j_e is the electron beam current density in [A/cm^2], τ is the ionization time in [s]), simulated according to the equation (2.12) with the use of the CBSIM code (Bro89) (Simulation result obtained at JINR, Dubna) with electron beam energy E_e = 5.6 keV.

The solution of the results obtained from equation (2.12) are represented on figure (3). Krypton charge state evolution is presented for electron beam energy of E_e = 5.6 keV. Since the given electron beam energy is less than binding energy for Kr^{35+} and Kr^{36+} (over 17 keV), the evolution saturates at charge state Kr^{34+} (binding energy 4.1 keV). Note that in the final charge state distribution the maximum possible (for a given electron beam energy) charge state Kr^{34+} is only 58%. There are some reasonable fractions of $Kr^{33+}$and Kr^{32+}caused by radiative recombination, as expressed in the radiative recombination's term in equation (2.12). This simulation displays the charge state evolution at the conditions that are very close to those achieved in ESIS Krion-2 (JINR, Dubna), when Kr^{27+} was produced and further used for irradiation of HOPG surface, as described in Chapters 3 and 5 of this Thesis. One should note that, according to the given results, when the Kr^{27+} charge state reaches its maximum value of about 30%, there are some reasonable fractions of a few neighbouring charge states Kr^{25+}, Kr^{26+}, Kr^{28+} and Kr^{30+}. This is a typical charge state spectrum of highly charged ions produced with EBIS and ESIS by electron impact successive ionization.

2.2.6 ION EXTRACTION

Ions are extracted from the trap in the axial direction by the creation of an appropriate distribution of potentials along the beam. There are three modes of ion extraction that can be used, and they are as follows:

- Ion extraction can be passive, when the right hand barrier is removed and ions leave the trap by virtue of their kinetic energy. In the self-consistent field model, the axial gradient of the field appears in the direction of extraction. If passive extraction is used, the energy spread of the ions outside the trap is the same as inside the trap. This lead to $0 < E_i < |s^-|\left(2ln\frac{R}{r_0}+1\right)$. The extraction time τ_{ex} is different for different cases. This can take the transit time for ions with charge state q and mass M through the length of the trap L in the electric field of gradient:

$$\frac{\partial U}{\partial Z} = |s^-|\left(2ln\frac{R}{r_0}+1\right)/L \qquad (2.13)$$

as being normally applicable for τ_{ex}. The extraction time is determined as

$$\tau_{ex} = \left[\frac{2M}{q}\frac{L^2}{|s^-|\left(2ln\frac{R}{r_0}\right)+1}\right]^{1/2} \qquad (2.14)$$

For example, if q / M = 0.5, I_e = 1A, R / r = 10, E_e = 10 keV, L = 100 cm then we get

τ_{ex} = 10^{-5}s = 10 µs. This is a typical extraction time of an ion pulse from EBIS/ESIS.

- The energy spread of ions outside the trap is made very small by a slow change in the potential distribution, when the right hand barrier is constant and the level of the bottom of the trap is increased slowly. More information can be viewed (see figure 12.5 (b)) in the book by Brown and Keller [Bro89].
- For fast active extraction that occurs when the distribution is transformed by the rapid application of external field $\frac{\partial U}{\partial z}$ along the system, the equation below estimates the extraction time when the electric field is applied instantaneously:

$$\tau_{ex} = \left(\frac{2M}{q}\frac{L}{\frac{\partial U}{\partial z}}\right)^{1/2} \tag{2.16}$$

Fast extraction allows a reduction in the extraction time to a few µs. There are several methods of producing ions. We proceed hereunder to discuss the second method in detail for electron string ion sources below.

2.3 ELECTRON STRING ION SOURCE (ESIS)

It is well known that EBIS-type ion sources produce the highest pulsed currents of highly charged ions, whilst the average ion beam intensity is relatively low. It is possible to increase the electron beam current as one method of increasing EBIS ion output and its density. For the purpose of avoiding a virtual cathode formation limit with its natural instability, it is necessary also to increase the electron beam energy. Such an uncomplicated method would lead to very high dissipated power of an electron beam, with the possibility of reaching hundreds kW or MW. Once achieved, it can be more or less convenient in the pulse and recuperation modes of operation.

The reflex mode of EBIS operation is one of the alternatives mentioned above. This constitutes the simplest method of increasing an ion yield. On the strength of the original construction of the electron gun and of the electron reflector in JINR, Dubna, the study of the reflex mode of EBIS operation was made possible [Don96a]. In principle, the purpose of the operation was to use multiple injected electrons which lead to the construction of the electron beam ion source operated in the reflex mode.

In this source the electrons restricted in a high magnetic field perform around 1000 oscillations between the electron gun and reflector. It causes the production of heavy electron

plasma at a low current to release electrons from the cathode. Thus, the dissolute electron power is reduced by 2-3 orders of magnitudes at a similar electron density in the reflex ion source. In these circumstances, the pure electron plasma of one component contains multiply reflected electrons that are compacted in a strong solenoid magnetic field which displays the properties related to a phase transition. The phase transition goes via powerful instability [Don04b]. This leads to appreciable electron energy spread which can subdue the instability. The phase transition can cause stepwise that increased the compacted density of the electron plasma in the new steady state so called the electron string [Don96b][Don98][Don99].
The electron string state is a stationary state of a hot pure electron plasma, which is heated by the injected electron beam and cooled by electron losses (mostly transverse) [Don04b].

An electron string is a state of one component electron plasma, which can arise when there is an accumulation of multiply reflected electrons in a strong solenoidal magnetic field [Don00a]. Both the electron string ion source and electron beam ion source are utilized for confinement and ionization of positive ions by electron collision to highly charged states [Don04b]. During the last decade the physics of electron strings was investigated in several laboratories in the JINR framework (Dubna, Russia), BNL (Upton, NY, USA), MSL (Stockholm, Sweden), and IAP (Frankfurt, Germany) in collaboration [Don00c][Don01].

Ion production through the application of electron strings instead of electron beams allows a saving of about 99 % of electric power of electron beam and simultaneously improves the reliability of an ion source considerably [Don04b]. The year 2002 saw ESIS Krion-2 (JINR) being used for the production of Ar^{16+} ion beams and their acceleration in the superconducting JINR synchrotron nuclotron. In this run on the accelerator facility, the ESIS "Krion-2" produced up to 150 μA of Ar^{16+} in a pulse of about 8 μs (i.e. 5×10^{8} Ar^{16+} ions per pulse), which was suitable for a single turn injection into the synchrotron. The slow extracted 1 GeV/n beams of Ar^{16+} ions were used for test physics experiments. In 2003, ESIS "Krion-2" produced 150 μA of Fe^{24+} in a pulse of about 8 μs (10^{8} Fe^{24+} ions per pulse) and the iron ions were accelerated to relativistic energies with JINR Nuclotron synchrotron [Don02][Don04b].

Various aspects of multi-charged heavy ions production benefitted from the use of the electron string ion source (ESIS) Krion-2 (JINR, Dubna) for basic and applied research [Don10]. Energy recuperation of an electron beam injected into an electron string was proved first and used for the production of highly charged ions like ($^{84}Kr^{27+}$ - $^{84}Kr^{32+}$),

($^{124}Xe^{40+}$ - $^{124}Xe^{44+}$) and (Au^{51+} - Au^{54+}) [Don10]. During the Nuclotron run №41 in February-March 2010, Krion-2 ESIS was applied on the high voltage platform of linear accelerator (LU-20) and used as an injector of highly charged ions.

Formatted: German (Germany)

One can summarize that ion yields produced by Krion-2 ESIS on HV platform of the linear accelerator during a Nuclotron run during the period spanning February-March 2010 was as expressed in the following table 2.1 [Don10]:

Table 2.1: Production of highly charged ions.

Highly Charged Ions	**Ions Per Pulse**	**Duration (μs)**
$^{84}Kr^{27+}$ - $^{84}Kr^{28+}$	3.5×10^7	7
$^{84}Kr^{29+}$	3.2×10^7	7
$^{84}Kr^{30+}$	3.0×10^7	7
$^{124}Xe^{41+}$	3.0×10^7	7
$^{124}Xe^{42+}$	3.0×10^7	7
$^{124}Xe^{43+}$	2.7×10^7	7
$^{124}Xe^{44+}$	1.5×10^7	7

Physics experiments were conducted using extracted Xenon beams, an injection of 3.0×10^7 $^{124}Xe^{42+}$ ions per pulse of 7 μs duration extracted from Krion-2 ESIS into LU-20 and into Nuclotron, then accelerated up to the energy 186 GeV.

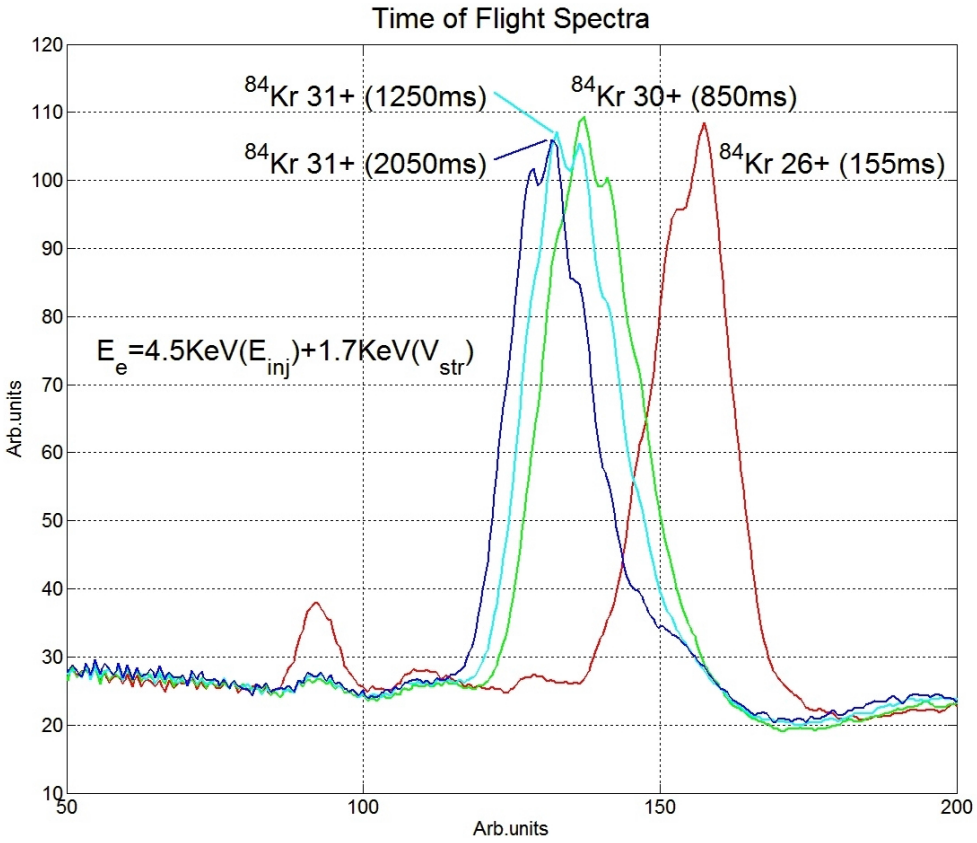

Figure 2.4: Time of flight charge state spectra of ^{84}Kr highly charged ions, created with Krion-2 ESIS at different ion confinement times. Electron injection energy was E_{inj} = 4.5 keV and drift tube structure was additionally lifted up to U_{str} = +1.7 keV [Don10].

Running for an estimated 30 days on HV platform, the electron string ion source Krion-2 demonstrated properties of high reliability and stability [Don10]. It is believed that it is due to the very low electron beam power, provided by utilization of the electron string (reflex) mode of operation (10 – 50 W pulse power) [Don10]. As a result, the electron string ion source of highly charged ions has become a new and useful tool for accelerator facilities and for basic and applied research with HCI.

Electron string ion source concept first was realized in JINR with use of the “old” electron beam ion source (EBIS) Krion-2. Some minor adjustments were made and they are listed below:

- Instead of the electron collector in EBIS, electrons are captured by the anodes of an electron gun and an electron reflector, which have an original sophisticated construction;
- The electron reflector mirror is arranged symmetrically in respect to electron gun. The negative voltage applied to the reflector, reflects all electrons back, whereas ions are extracted outside through an orifice in the reflector on its axis.

The scheme of ESIS is very similar to EBIS, however the few differences mentioned above change the concept in a principal way.

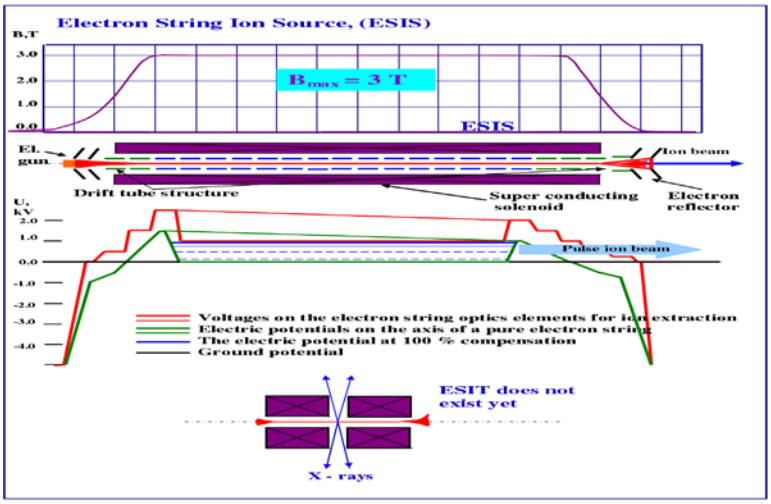

Figure 2.5: A schematic diagram of electron string ion source Krion-2.

The third method of ion production, which is the electron cyclotron resonance ion source will be discussed in the next section.

2.4 ELECTRON CYCLOTRON RESONANCE ION SOURCES

An electron cyclotron resonance ion source is based on a plasma which is held in an open magnetic trap [Bro89]. The plasma forming electrons and ions are created by electron impact ionization processes from neutral atoms or molecules. The emitted electrons are heated by the microwave field and participate in the further ionization of atoms or molecules. The ions are ionized to an extent where they are lost from the working area of the source. The ion charge state is determined by the density of the electron component and the lifetime of the ions in the plasma. Therefore, the maximum achievable charged state of the ions is

determined by the electron energy. There are some conditions for the production of very highly charged ions that are different from the electron beam ion sources. The charge exchange processes have no determining influence on the production of highly charged ions.

The MINIMAFIOS is an example of the ECR ion source and it is discussed below: ECR ion sources use electron impact for ionization. A typical electron cyclotron resonance ion source consists of a vacuum chamber, vacuum system, and a system of solenoids or permanent magnets which are used to create the required form of magnetic field. It also consists of a waveguide for providing the microwave radiation into the vacuum chamber and a system of dosed working gas injection alongside an extracting system and other devices.

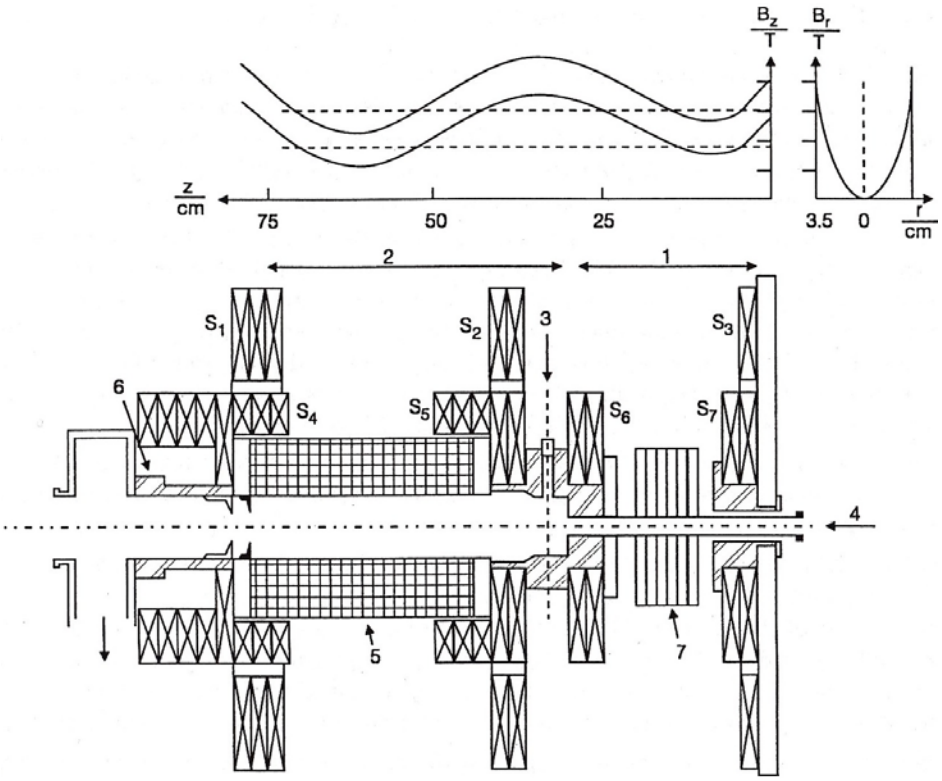

Figure 2.6: A schematic diagram of the electron cyclotron resonance ion source (ECRIS) MINIMAFIOS and magnetic field distridution, B_z along the axis and the B_r along the radius in the central part of the source [Gel87].

In the upper part, two horizontal dash lines correspond to the operation of the ion source at 10 GHz and at 16,6 GHz. In the lower part, the main elements of the ion source are presented: S_1, S_2,... S_7 – solenoid coils for the production of the axial magnetic field, 1 – low vacuum

stage of the source 2 – the main stage of the source, 3 – waveguides for the injection of the microwave radiation, 4 – gas injection channel, 5 –permanent magnets hexapole for the production of the radial magnetic field, 6 –ion extraction electrode system, 7 – cooling radiator [Gel87].

First, the theoretical basics of the ions production is described in section 2.4.1 under Electron impact ionization. Information about the main systems and important processes in a typical electron resonance ion source is presented in 2.4.2 Magnetic field confinement, 2.4.3 Electron cyclotron resonance heating, 2.4.4 Charge exchange loss, 2.4.5 Ion confinement, 2.4.6 The plasma injector stage and 2.4.7 Gas recirculation in ECR sources.

2.4.1 ELECTRON IMPACT IONIZATION

Ions are generated by a step by step ionization which is due to the impact of energetic electrons. The electron impact ionization cross section has to be a significant parameter. The following equation expressed the electron impact ionization to produce the rate of ions of charge state i:

$$R_{prod,i} = n_e \langle \sigma_{i-1,} v_e \rangle n_{i-1} \tag{2.17}$$

where n_e , $\langle \sigma_{i-1,} v_e \rangle$ and n_{i-1} represent the electron density and rate coefficient, and product of the electron collision ionization cross section with charge $(i-1)$ and i. The electron velocity v_e averaged above the electron energy distribution and the ion density charge state $(i-1)$ [Bro89].

2.4.2 MAGNETIC SYSTEM AND MAGNETIC FIELD CONFINEMENT

The density of the highly stripped ions is dependent on the electron impact ionization cross sections and the flux of the high energy electrons. The electron impact ionization cross section must have a small value while the flux of the high energy electrons must be reasonably large in order to produce a significant density of highly stripped ions.

An extremely large flux is required when the electrons are traveling through a system such as the electron beam ion source. To avoid the problems of using large flux, it is possible to confine the electrons and ions by forming neutral plasma. Each electron makes many passes through the system, and the dissipated power is essentially limited to the energy carried away by the flux of electrons escaping from the confinement region.

To confine the plasma, a special magnetic field configuration can be used. With this type of configuration, the magnetic field is usually at its minimum at the centre of the device. The important parameter of the confinement geometry is called the mirror ratio. This mirror ratio is the ratio of the maximum field strength at the magnetic mirrors to the field strength at the centre of the device. The minimum magnetic field configuration is produced by combining an axial field from solenoid coils with a multipole field that are either hexapole or octupole. Multipole fields are produced by coils or permanent magnets.

2.4.3 INJECTION OF THE WORKING GAS

A leak valve can be used to introduce the gas into the plasma area of the vacuum chamber of the electron cyclotron resonance ion source. It is possible to create ions of metals. For this purpose, a special oven, connected to the vacuum chamber, is used. The working substance is heated in the oven to a high temperature, evaporates and enters as a gas to the vacuum chamber of the ion source. If the ion source has two stages, the gas goes to the first stage with relatively high pressure, where it forms the plasma.

2.4.4 PLASMA INJECTOR STAGE

The Paschen law on avalanche discharge in gas shows that it is not possible to break down a neutral gas to form a plasma if the gas pressure is too low [Bro89]. For this reason the electron cyclotron resonance ion sources were developed as two stage devices. The first stage is a cold plasma generator operating at higher pressure. The plasma produced in the first stage flows along the magnetic field lines into the second stage. The flow is governed by the density gradient between the first and second stages.

2.4.5 ELECTRON CYCLOTRON RESONANCE HEATING

In order to optimize the rate of ionization by electron impact, electron temperatures between 1 and 10 keV are required [Bro89]. High ion temperature is required as the source of emittance to extracted beam. The method to heat electrons in the plasma is preferable. Electron cyclotron resonance heating remains a suitable method for heating electrons.

Charge particles (electrons or single positively charged ions) travel in the magnetic field B on spiral orbits with the following Lamour radius r_L given as:

$$r_L = \frac{Psin\theta}{ieB} \tag{2.18}$$

where P and θ are particle impulse and the angle between the directions of the magnetic field and the particle movement. The Larmour radius of electrons and ions are usually fractions of a millimetre.

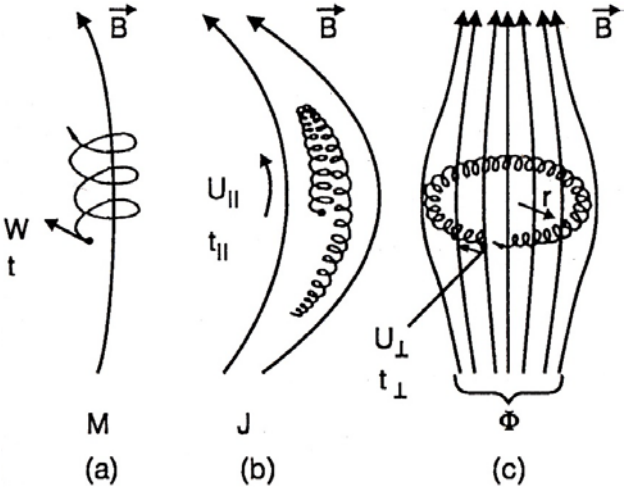

Figure 2.7: A schematic diagram showing the movement of charged particles in the magnetic field. (a) movement along a field line in the axial magnetic field, (b) reflection at the magnetic mirror, (c) azimuthal particle drift [Con78].

The progressive movement of the charge and the step of the spiral are determined by the velocity component parallel to the direction of the magnetic field. The rotation frequency ω_{ce} of the electrons in the magnetic field, called the cyclotron frequency, is given by:

$$\omega_{ce} = \frac{eB}{m} \tag{2.19}$$

The excitation processes are spread in the plasma with the eigenfrequency of the plasma ω_{pe} and are determined by the plasma density. The eigen frequency of the electrons in the plasma is determined by the following equation:

$$\omega_{pe} = \sqrt{\frac{4\pi n_e e^2}{m}} \tag{2.20}$$

Therefore, an electromagnetic wave is fed into the plasma in resonance with one of the frequencies shown in either equation (2.19) or (2.20). A combination of both equations can also be expressed as:

$$\omega = \sqrt{\omega_{ce}^2 + \omega_{pe}^2} \tag{2.21}$$

This can exchange energy with the electron component of the plasma. Cyclotron resonance is usually used for the plasma heating at the frequency as mentioned in the above equation (2.19) or, in some cases, through the hybrid resonance equation (2.21).

The electromagnetic wave has to be expanded in the plasma in order for it to effectively transmit energy to the electrons. Therefore, the frequency must be higher than the eigenfrequency of the plasma ω_{pe}. This condition limits the electron density in the plasma by the following equation:

$$n_e \leq \frac{\omega_{ce}^2}{4\pi r_e c^2} = 1.24 \times 10^{-8} f^2 \qquad (2.22)$$

where f is the plasma heating frequency in Hertz. The resonance condition at a given microwave frequency is fulfilled only at certain values of the magnetic field B_{res} which are determined from equation (2.19). For the design of the magnetic field of the ECR source, the value of B_{res} is calculated from the condition $B_{min} < B_{res} < B_{max}$ and where B_{min} indicates the minimal value of the magnetic induction in the centre of the magnetic trap and B_{max} is the maximum value of the field along the source axis.

The relationship of equation (2.22) indicates that an increase of the heating frequency can lead also to an increase of the maximum possible electron density. This can be one of the ways to perfect ECR sources of highly charged ions.

2.4.6 CHARGE EXCHANGE LOSS

There are two significant processes in which highly charged heavy ions can be lost from a plasma. These processes are loss of confinement and charge exchange with neutral atoms in the plasma. Charge exchange between highly charged ions and neutrals for cross sections are very large. The following equation expressed charge exchange from the initial charge state i to the final charge state $(i-1)$ of the cross section:

$$\sigma_{i,i-1} = 1.43 \times 10^{-12} i^{1.17} V_{0,1}^{-2.17} cm^2 \qquad (2.23)$$

where the $V_{0,1}$ represents the neutral atom of the first ionization potential (eV) [Bro89].

The charge exchange cross sections can be about four orders of a magnitude larger than the ionization cross sections of the electrons [Bro89]. The reaction rates which are proportional to the projectile velocity and neutral atoms are much slower than in hot electrons. In order to

retain the creation rate by electron impact equal to the loss rate by charge exchange for high state ions, it is required for the neutral atom density to be two orders of magnitude lower than the electron density [Bro89].

2.4.7 ION CONFINEMENT

This is the second mechanism of the loss of confinement for beam extraction. An electron cyclotron resonance ion source differs from electron beam ion source in that it is not possible to stop the ion confinement to extract the confined ions.

Here all extracted ions have undergone a loss of confinement. These ions are available for extraction to the extent that they are lost axially from the confinement region and stream toward the ion extractor. The ion confinement time is a critical parameter in electron cyclotron resonance ion sources. If the time of restriction is too short, the ions do not have enough time to reach high charge states [Bro89]. If the restriction is too long, the high charge state ions decay by charge exchange instead of being separated [Bro89]. The mechanism of ion confinement is not clearly understood. The plasma potentials caused by the ambipolar diffusion are present, but are probably very small.

2.4.8 GAS RECIRCULATION

The imperfect confinement of the plasma leads to the continuous escape of an ion flux from the plasma. Only a small fraction of the flux, which escapes along the source axis, reaches the extraction hole and is accelerated as a beam. Most of the ion flux hits the walls where ions are neutralized or scattered elastically back into plasma. This wall appears as an intense source of neutral gas. The neutrals generated at the walls are re-ionized by the plasma or evacuated by the system of the vacuum pumps. In electron cyclotron resonance ion sources, the plasma pumping speed is much larger than the pumping speed of the external pumps. These means that each ion undergoes several plasma wall cycles before escaping the system as an accelerated beam or as neutral gas evacuated by the vacuum pumps.

2.5 REFERENCES

[Bro89] I. G. Brown and R. Keller. "The Physics and Technology of Ion Sources" John Wiley & Sons 2 (1989) 207-278.

[Con78] R. H. Conen, M. E. Rensink, T. A. Cutler, A. A. Mirin. "Nuclear Fusion" 18 (1978) 1229-1243.

[Don77] E.D.Donets. "Proceedings Fifth All-Union Conference on Charged Particle Accelerators" Nauka Moscow 1 (1977) 346-347.

[Don90] E. D. Donets. "Electron Beam Ion Sources and Their Development at JINR" Review of Scientific Instruments 61 (1990) 225-229.

[Don96a] E. D. Donets, D. E Donets and E. E. Donets. "Patent RU2067784" Bull. IZOBRETENIA, Moscow 27 (1996) 1-4.

[Don96b] E. D. Donets. "Review of Recent Developments for Electron Beam Ion Sources (EBIS)" Review of Scientific Instruments 67 (1996) 873-877.

[Don98] E. D Donets. "Historical Review of Electron Beam Ion Sources" Review of Scientific Instruments 69 (1998) 614-619.

[Don99] E. D. Donets, D. E. Donets, E. E. Donets , V. V. Salnikov and V. B. Shutov. "Evolution of Argon K X-ray Spectra during the Ion Confinement in Electron String" Physica Scripta T80 (1999) 500-501.

[Don00a] E. D Donets. "Electron Beam Ion Sources in the Reflex Mode of Operation (Review And Progress Report)" Review of Scientific Instruments 71 (2000) 810-815.

[Don00b] E. D. Donets, E. E. Donets and E. M. Syrensin. "Theory and Simulations of lectron Beam Ion Sources in Reflex Mode" Review of Scientific Instruments 71 2000) 887-889.

[Don01] E. D Donets, D. E Donets and E. E Donets et al. "Electron Beam Ion Sources and traps and Their Applications" 8th International Symposium, BNL USA, AIP Conference Proceedings 572 (2001) 103-118.

[Don02] E. D Donets, D. E. Donets, E. E. Donets, V. V. Salnikov, V. B. Shutov, Yu A. Tumanova, V. P. Vadeev et al. "Electron String Source of Highly Charged Ions: Studies and the First Test on a Synchrotron" Proceedings of EPAC-2002, Paris 73 (2002) 1700-1702.

[Don02] E. D Donets, D. E. Donets, E. E. Donets, V. V. Salnikov, VB Shutov, Yu A. Tumanova,V. P. Vadeev et al. “Status Report on Studies of EBIS in the String Mode of Operation” Review of Scientific Instruments 73 (2002) 679-681.

[Don04a] E. D Donets, D. E. Donets, E. E. Donets, V. V. Salnikov, V. B. Shutov, S. V. Gudkov, Yu A. Tumanova, and V. P. Vadeev. “Use of EBIS in the String Mode of Operation on the Nuclotron Facility in JINR” Review of Scientific Instruments 75 (2004) 1543-1545.

[Don04b] E. D Donets. “Electron String Phenomenon: Physics and Use” In Journal of Physics: Conference Series. IOP Publishing 2 (2004) 213-219.

[Don10] D. E Donets, E. D. Donets, E. E. Donets, V. V. Salnikov, and V. B. Shutov. “Production of Highly Charged Ion Beams Kr^{32+} , Xe^{44+} , Au^{54+} with Electron String Ion Source (ESIS) Krion-2 and Corresponding Basic and Applied Studies”Journal of Instrumentation 5 (2010) 1-18.

[Gel87] R.Geller, F.Bourg, P.Briand et al. “Proceedings of the International Conference On ECR Ion Sources” NSLC-Report MSUCP-47 East Lansing USA 1 (1987)1-32.

[Ger05] F. Gerd. “Physics of Electron Beam Ion Traps and Sources”IEEE Transactions on Plasma Science 33 (2005) 1763-1777.

[Her58] G. J. Herrmann. “Optical Theory of Thermal Velocity Effects in Cylindrical Electron Beams” Applied Physics 29 (1958) 127-127.

[Lot67] W. Lotz. “Ionization Potentials of Atoms and Ions From Hydrogen to Zinc” JOSA 57 (1967) 873-877.

CHAPTER 3: INSTRUMENTATION

This chapter describes the instruments used in this study of interaction of highly charged ions with solid surfaces. The main instruments used in this research are the electron string ion source (ESIS) Krion-2 (Veksler-Baldin Laboratory of High Energy Physics, JINR) and the electron cyclotron resonance ion source (ECR) in the Flerov Laboratory of Nuclear Reactions, JINR. In this chapter we shall discuss in detail the most important parameters of the Krion-2 ESIS (3.1) and of an electron cyclotron ion source (3.2).

3.1 ELECTRON STRING ION SOURCE (ESIS)

The physics principles and technical description of the Krion-2 ESIS (JINR) were described in previous chapter in section 2.3. Now we add some important details.

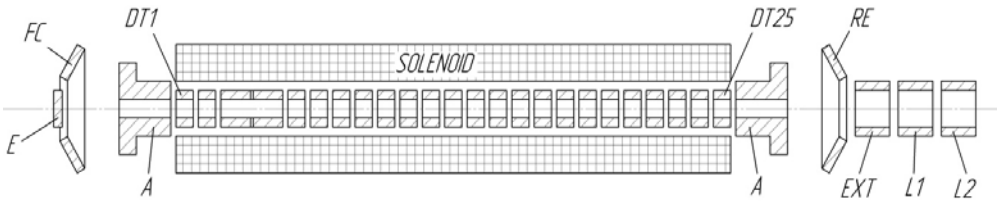

Figure 3.1: A schematic diagram of the Krion-2 ESIS: (a) electron emitter (E), (b) false-cathode electrode (FC), (c) surrounding emitter, (d) anodes (A) (electron gun anode –left, electron reflector anode – right), (e) sectioned cylindrical drift tubes (DT1-DT25) are arranged inside the bore of a superconducting solenoid with $B_{max} = 3$ Tesla, (f) electron reflector (RE) with an orifice at the centre for the ions extraction; (g) focusing electrostatics lenses (EXT,L1 and L2) for ion beam extraction and focusing. The total length of the ionization trap between DT1 and DT25 is 120 cm. The axial symmetry and geometrical axis of the system coincides with the magnetic axis of the solenoid with a precision better than 0.1 mm.

The electrons are emitted from a Ce-metal-alloy cathode (cathode diameter is 1 mm) and are accelerated electrostatically up to few keV in the cathode-anode gap. A negative potential is applied to the cathode while the; anodes and drift tubes are usually at a ground potential. One can additionally apply some positive potential on drift tubes in order to increase the electron energy. The electron gun is a pierce-like gun with false-cathode focusing electrodes arranged

at the pierce angle 22.5 degree from the vertical. The emitter is arranged at the fringe of the magnetic field of the superconducting solenoid at $B_{cathode}$ = 1 / 20 B_{max}; thus the electron beam is a magnetically compressed in $\sqrt{20}$ times when penetrating into the uniform magnetic field region where $B = B_{max}$.

Ions are trapped inside the drift tubes (between DT1 and DT25) when liquid helium temperature is about 4.5 K. Therefore, this happens when the vacuum conditions reach 1.33×10^{-11} mbar in the ionization trap region, since the cold drift tubes work as a cryogenic pump permanently. Vacuum conditions at the electron gun and electron reflector regions are in a range of 1.33×10^{-7} mbar. The gun and reflector regions are at room temperature during ESIS operation, whereas the temperature of the Ce-metal-alloy emitter is 1800 ^{0}C. After passing through the drift tube structure, electrons are reflected by the negative potential applied to the electron reflector (negative potential at the electron reflector is usually in two times more negative than in cathode, thus all electrons are reflected from it). As a result, electrons return back into the drift tube structure region and then they are completely reflected back again by the cathode potential. The reason for their reflection from cathode potential (where they were born) is that the electrons get some transversal velocity at each reflection and hence cannot reach the cathode surface after it. At some conditions the conglomerate of multiple reflected electrons form a steady state with an increased efficient current density. This state is the so called electron string. The electron string is formed in the Krion-2 ESIS with the emitted current of 0.1 A. The corresponding efficient electron current density was in the range of 200 – 500 A/cm^2. This corresponds to an average lifetime of each electron of about 200-300 oscillations through the ESIS drift tube structure. After many longitudinal oscillations, electrons escape the trap in a radial direction across the magnetic field and are captured by anodes. In this steady electron string state one can produce highly charged ions similar to the electron beam as (in EBIS).

Gaseous working species, such as krypton, is injected as a neutral atom gas inside the drift tube space at the border between room temperature and cryogenic temperatures (section DT2-DT3). Neutral atoms become singly ionized when crossing, once the electron string and then ions are trapped radially by the electron beam potential and axially by electrostatic positive potentials of a few kV, applied at the end sections of drift tube (DT1, DT25). Details of the injection and ionization procedures are described in chapter 2. When the desired mean ion

charge state is reached, the potential at the drift tube section (DT25) drops, at the same time potentials of other drift tube sections can be lifted up to 1.5 kV. This allows the ions to escape towards the electron reflector. The negative voltage applied to the electron reflector, acts as an extraction voltage for an ion beam. As a result, the produced ion beam with mean charge state q+ has a kinetic energy up to q^+ x 1.5 kV. The extracted ion beam then can be focused by three electrostatic lenses (EXT, L1 and L2) and then it enters to the time-of-flight (TOF) charge/mass spectrometer which allows for obtaining the charge state spectra of the produced ion beam.

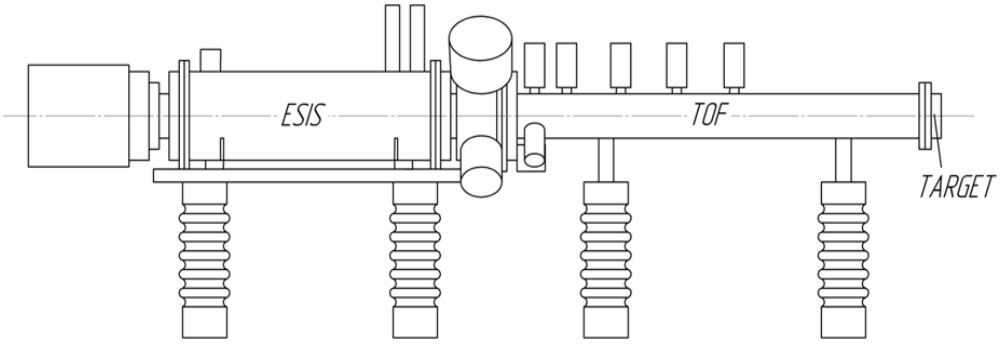

Figure 3.2: A schematic diagram showing the experimental set-up: (a) Produced HCI ions in drift tube of the KRION-2 ESIS travelling through the time-of-flight charge-to-mass spectrometer (TOF) to the target. The produced ion beam does not get any additional acceleration/deceleration inside the TOF. One can apply some positive voltage on a target in order to reduce kinetic energy of the ions to a possible minimum value.

Electron string ion sources measurements are described and discussed in chapter 5.

3.2 ELECTRON CYCLOTRON RESONANCE (ECR) ION BEAM

Electron cyclotron resonance ion sources have been used in plasma fusion developments in 1960 [Bro89a]. In 1969, the employ of electron cyclotron resonance heating in plasma instruments was suggested to create high charge state ions. The creation of multi-charged ions with electron cyclotron resonance heating was investigated by Geller in France and Wiseman in Germany in 1972 [Bro89b]. The plants were very large, expensive and energy consuming [Bro89c]. Electron cyclotron resonance ion source (ECRIS) is now employed for the creation of high quality multi-charged ions beam for accelerator, atomic physics and industrial applications. The work reported in this research was performed using electron cyclotron resonance ion sources in Flerov laboratory of Nuclear reactions at the Joint Institute

for Nuclear Research (JINR). Schematic diagrams of the cyclotron resonance ion source are represented in figures 3.3 and 3.4, respectively.

In electron cyclotron resonance ion source, multi-charged ions are produced by a step by step ionization method induced by the collision of energetic electrons. Energy of 50 keV was used to irradiate the highly oriented pyrolytic graphite samples. The electron cyclotron resonance ion source used in this experiment is described below in section 3.2.1.

3.2.1 THE ECR USED FOR SAMPLE IRRADIATION

Ions for sample irradiation were produced by the one stage normal conductivity ECR with hexapole magnetic field configuration. The main parts of ECR shown in the figure 3.4. are: AM – water cooled solenoids producing axial magnetic field, RM – permanent magnets producing hexapole magnetic field, GI – gas inlet for connecting the ECR ion source to the source of neutral working substance, MI – microwave inlet to guide the microwave radiation from the supply to the plasma chamber P, where the electron cyclotron resonance heating of the plasma takes place. EXT – the extracting electrode under high negative potential extracts and forms the beam.

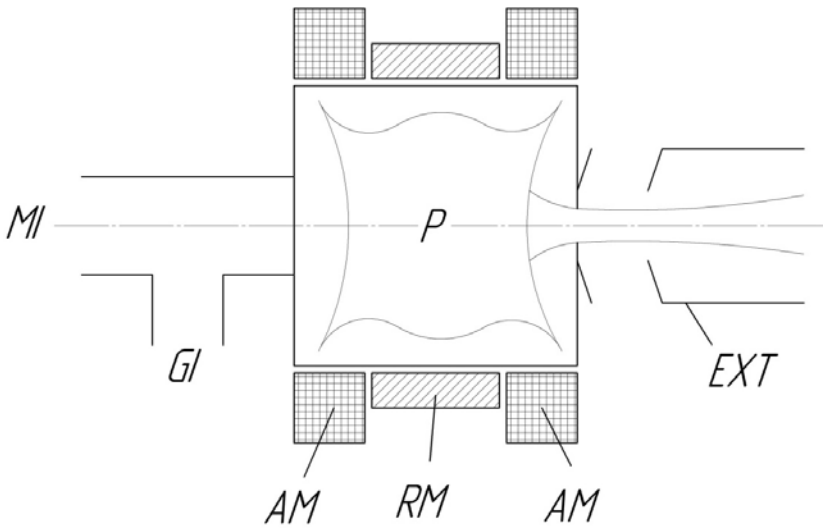

Figure 3.3: A schematic diagram of ECR.

The axial magnetic field is formed by two separate water cooled coils with an iron yoke and the radial magnetic field is formed by a permanent magnet hexapole. The hexapole is made from 24 identical magnet elements with a defined direction of a magnetic induction. The magnetic elements form a strong magnetic field inside of the plasma chamber. An inlet system (GI) for gasses and solid substance is situated at the inside of the device. There are two method used for the inlet system for solid materials, viz., metal ions from volatile compounds or a mini-oven. There are current supplies for the mini-oven and the positional inlet system. The mini-oven warms the solid substance and the material vapours diffuse to the plasma where they are ionized. The maximum temperature in the mini-oven was 110 ^{0}C. The microwave frequency and the maximum power were 14 GHz and 2 kW, respectively. The ions are extracted from the ion source by a plasma electrode of a cylindrical symmetry and afterwards are formed to the ion beam of required parameters. The minimum extraction ion source voltage was 30 kV.

3.2.2 ECR TEST SETUP

The HOPG target was irradiated with electron cyclotron resonance (ECR) ion source. This is the low energy beam transport system designed for research. The ECR test setup is shown schematically in the figure 3.3. It consists of: ECR- the electron cyclotron ion source, EB – extracting box, FS – focusing solenoid, AM –analysing magnet, QM – quadrupole magnet, DB – diagnostic box and TB – target box.

The ECR ion source producing the ions is the first part of the beam line. The extracting box has the extracting electrode, which serves to extract the ions and form the beam. Also, it has a port for a high vacuum pumping system. The focusing solenoid is the part of ion optics of the ECR test setup. The axis of the magnetic field created by this solenoid coincides with the axis of the ion beam. The analysing magnet is the dipole magnet with the axis of the created magnetic field perpendicular to the axis of the ion beam. It bends the beam in the horizontal plane. The mass spectrum analysis is obtained by using the magnet that focuses the beam. The quadrupole magnet is the magnet focusing the beam to the proper condition on the diagnostic equipment and the target. The diagnostic box contains the parameters for measuring the condition of the ion beam. Using this information precisely enough, one can calculate the time and the number of ions irradiating the target. The target box has a high vacuum pumping system. This can be disconnected from the diagnostic box using the gate valve to load or unload the target, without affecting the vacuum in the beam transport line and in the electron cyclotron ion source. At this condition the target box was opened to mount

the HOPG target inside. Then the target box connected to the diagnostic box was evacuated and the HOPG target was irradiated.

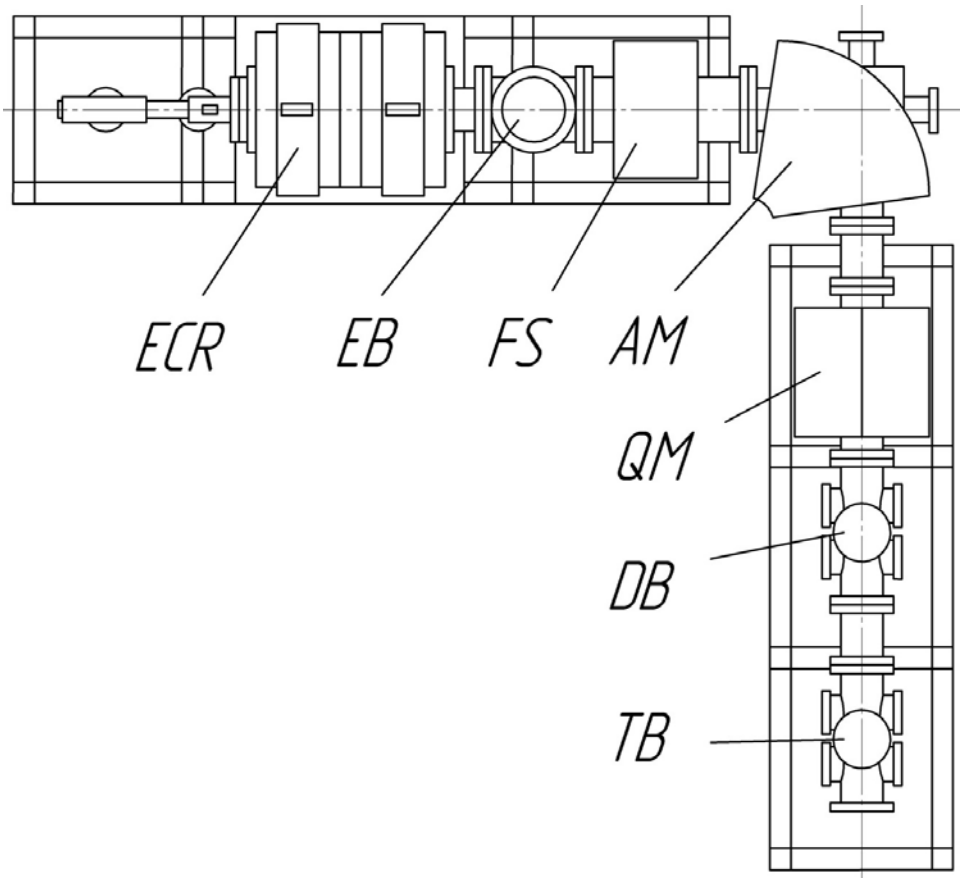

Figure 3.4: A schematic diagram of electron cyclotron resonance ion sources test setup.

Electron cyclotron resonance ion sources measurements are described and discussed in chapter 5.

3.3 SCANNING PROBE MICROSCOPY(SPM)

In the early 1980s, scanning probe microscopy was developed to investigate surfaces with atomic resolution. Gerd Binnig and Heinrich Rohrer are acknowledged to be the founders of the SPM. They invented the first scanning tunnelling microscope in 1981 while working at IBM's Zurich research centre [Tau03]. The discovery made by Gerd Binnig and Heinrich Rohrer of SPM was a great breakthrough in the field of nanotechnology. Scanning probe microscopy has since then become a powerful tool to see individual atoms, to manipulate

atoms to build different structures and study their properties. SPM operates in different kinds of modes such as scanning tunneling microscopy mode and in atomic force microscopy mode. Scanning probe microscope set up and mechanics will be discussed below (3.3.1). The main focus of this study was to use the scanning tunnelling microscope mode of SPM. The basic principles of STM will be discussed in more details (3.3.2).

3.3.1 SCANING PROBE MICROSCOPE SETUP

Scanning probe microscope consists of several parts (see figure 3.6 and 3.7): the metal tip, the piezoelectric manipulator or actuator which is used to drive the metal tip relative to the sample. The sample is fixed to the microscope basement. The z-control and xy-control electronics which include the following:

- tunneling current converter
- analog to digital (ADC)
- digital to analog (DAC) conversion electronics.

It also contains high voltage amplifiers and the digital signal processing (DSP) board to evaluate the feedback signal from the computer that process the data and provides user interface. The sample landing system of the microscope consists of a stepper motor with a reduction gear. The microscope has two changeable measuring heads, one for operation in tunneling mode and other for operation in atomic force mode.

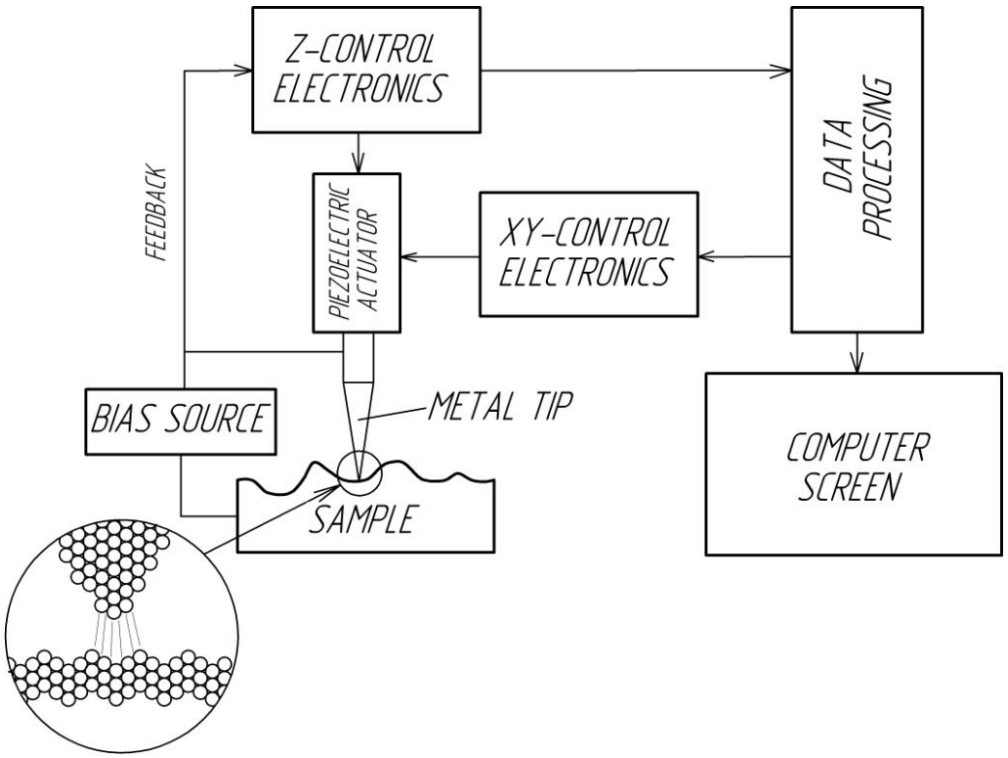

Figure 3.5: A schematic diagram of scanning tunnelling microscope [www1].

A scanning probe microscope system is shown in figure 3.6 below. The main processing computer has additional devices.

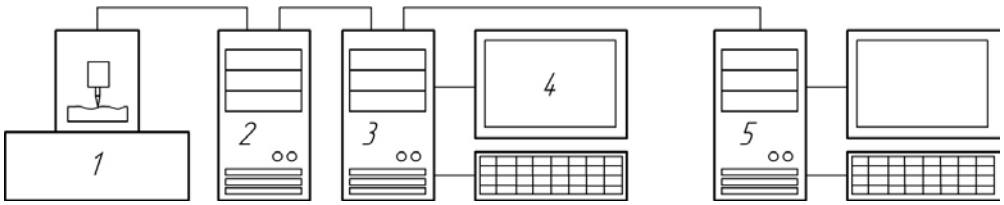

Figure 3.6: A schematic representation of scanning probe microscope system: (1) microscope, (2) control computer with following devices: DAC and ADC conversion unit, stepper motor controller and DSP board, (3) local image processing server computer with the monitor 4, (5) computer of remote user [Fil11].

3.3.2 SCANNING TUNNELLING MICROSCOPE OPERATIONS

The microscope has two changeable heads as discussed above (3.3.1), it can operate in two modes such as scanning tunnelling mode and atomic force mode. In this research, the

measurements have been carried out in the constant tunnelling current mode. The principle of the scanning tunnelling microscope is based on tunnelling current in the middle of the probe tip and highly oriented pyrolytic graphite sample to sense the features of the highly oriented pyrolytic graphite (HOPG).

The scanning tunnelling microscope was placed a few atomic diameters over highly oriented pyrolytic graphite which was a conducting material and electrically biased with respect to the probe tip. Below 1nm distance, a tunnelling current moves from HOPG to the probe tip. The voltage bias are in the range of 10 - 1000 mV as the tunnelling current typically change from 0.2 - 10 nA. The tunnelling currents transforms exponentially with the probe tip sample separation. There are typical decreases by a factor of 2 while the separation was increased by 0.2 nm. The instrument is digitally controlled, which is capable of producing high resolution and three dimensional images.

The samples are held in position as a piezo crystal in the form of a cylindrical tube scans the sharp metallic probe above the surface in a raster pattern. The digital signal processor determined the needed separation probe tip from the sample by sensing the tunnelling current moving in the middle of the sample and the probe tip. The voltage bias employed to the sample allows the tunnelling current to move. The DSP finishes the signal feedback loop by outputting the needed voltage to the piezo tube. The scanning tunnelling microscope (STM) can be operated in two modes as mentioned above.

In one case the gains of the feedback were put high, the tunnelling tips nearly tracks the surface sample and the variations in the height need to retain constant tunnelling current was determined by the alter in the voltage used to the piezoelectric tube. In the other case, the gains of the feedback were put low, the tip retains at a closely constant height while it sweeps above the surface sample and the tunnelling current was imaged.

For both samples we have started by obtaining 10 x 10 nm^2 low resolution images. This was the origin of the HOPG samples surface for low resolution images. There was nothing on the images. The following high resolution images 350 x 950 nm^2, 400 x 600 nm^2, 500 x 500 nm^2 and 2000 x 2000 nm^2 respectively was collected for HOPG samples irradiated with Kr^{27+} ions in this experiment. And also for HOPG samples irradiated with Ti^{5+} ions the high resolution images was 500 x 650 nm^2 and 700 x 700 nm^2 respectively.

The STM techniques have their own requirements. They can use all materials but have to be conductive. In this project we have used a highly oriented pyrolytic graphite sample, which

was conductive as the requirement for STM. The metal tip must be brought close to the sample at a distance of few Ångström which determine the resolution of the technique. It also allows the electron tunnelling to occur. It must have vibration isolation. The sample has to be clean and it must be placed inside a container to avoid contamination.

In order to obtained good resolution it is important to control the distance between the probe and the samples. The probe must not crush the samples. Good results can be obtained using high frequency noise filtering and to increase an image contrast.

The scanning tunnelling microscope is able to provide information in the following conditions [www2]:

- To acquire atomic scale images of metal surfaces.
- To reveal surface defects.
- Provides a three dimensional profile of the surface which is very useful for characterizing surface roughness.
- To determine the size, conformation of molecules and aggregates on the surface.
- To move individual atoms as well as to generate high resolution maps of material surfaces.
- The study of conduction or charge transport mechanisms.

3.3.3 MICROSCOPES USED IN THIS STUDY

Femtoscan and Nanoscope scanning tunnelling microscopes were used to analyse the surface atomic structure of HOPG samples irradiated with krypton and titanium ions. Femtoscan scanning probe microscope at Lomonosov Moscow State University in Advanced Technologies Centre was used. The image mode that was used for femtoscan scanning probe microscope was constant tunnelling current mode. Femtoscan software was used to control and to process images acquired by the microscope.

The picture of the microscope at Advanced Technologies Centre in Lomonosov Moscow State University used in this research is presented on figure 3.7.

Figure 3.7: The FemtoScan microscope at Advanced Technologies Centre in Lomonosov Moscow State University.

Further investigation was done with Nanoscope scanning tunnelling microscope employed at the University of Pretoria. Nanoscope software was used to process and analyse the surface morphology of highly oriented pyrolytic graphite. Constant tunnelling current mode was used to analysed the samples.

The results of scanning tunnelling microscope will be analysed and discussed in more details in chapter 6.

3.4 REFERENCES

[Bin83] G. Binning, H. Rohrer. "Scanning Tunneling Microscopy" Surface Science 126 (1983) 236-244.

[Bog10] S. Bogomolov, A. Efremov, V. Loginov, A. Lebedev, N. Yazvitsky, V. Bekhterev, Yu Kostukhov et al. "Present Status of FLNR (JINR) ECR Ion Sources" Beam Dynamics Newsletter 53 (2010) 1-55.

[Bro89] I. G. Brown. "The Physics and Technology of Ion Sources" John Wiley & Sons 2 (1989) 207-278.

[Che93] C. J. Chen. "Introduction to Scanning Tunneling Microscopy" New York: Oxford University Press 227 (1993) 1-26.

[Don02] E. D. Donets, E. E. Donets and D. E. Donets. "Tubular Electron Beam Ion Source" Review of Scientific Instruments 73 (2002) 696-698.

[Don04] E. D. Donets. "Electron String Phenomenon: Physics and Use" Journal of Physics: Conference Series. IOP Publishing, 2 (2004) 213-219.

[Don07] D. E Donets, E. D. Donets, E. E. Donets, V. M. Drobin, A. V. Shabunov, Yu A. Shishov, V. B. Shutov et al. "Design of a Novel Tubular Electron String Ion Source (TESIS)" MOPC 141 (2007) 403-405.

[Fil11] A. S Filonov, I. V. Yaminsky. "Scanning Microscope Probe Image Processing Software User's Manual FemtoScan" Version 2.2.90. Advanced Technologies Centre Moscow 1 (2011) 1-82.

[How96] R. Howland and L. Benatar. "A Practical Guide: To Scanning Probe Microscopy" Park Scientific Instruments. Sunnyvale CA 1 (1996) 1-87.

[Sak04] M. Sakurai, F. Nakajima, T. Fukumoto, N. Nakamura, S. Ohtani and S. Mashiko. "Design of EBIS for Nanoprocesses Using HCI" in Journal of Physics: Conference Series. IOP Publishing 2 (2004) 52-56.

[Tau03] M. Taub, B. Menzel, G. Khanna, and E. Lilleodden. "SPM Training Manual" Laboratory for Advanced Materials Stanford University 2 (2003) 1-15.

[www1] http://esperia.iesl.forth.gr/~ujonas/.../lecture_IntroSurfChem_2a_2.pdf, 19th August 2014.

[www2] http://physics.nist.gov/GenInt/STM/text.html, 19th August 2014.

[Xie98] Z. Q. Xie. "Production of Highly Charged Ion Beams from Electron Cyclotron Resonance Ion Sources" Review of Scientific Instruments 69 (1998) 625-630.

[Xik04] Z. Xikai, J. Dikui, G. Panlin, S. Shugang, Y. Heping, G. Peirong, W. Naxiu et al. "Shanghai Electron Beam Ion Trap: Design and Current Status" In Journal of Physics: Conference Series. IOP Publishing 2 (2004) 65-74.

[Zsc08] G. Zschornack, M. Kreller, V. P. Ovsyannikov, F. Grossman, U. Kentsch, M. Schmidt, F. Ullmann, and R. Heller. "Compact Electron Beam Ion Sources/Traps: Review and Prospects" Review of Scientific Instruments 79 (2008) 02A703-5.

[Zsc09] G. Zschornack, F. Grossmann, V. P. Ovsyannikov, R. Heller, U. Kentsch, M. Kreller, M. Schmidt, A. Schwan, A. Silze, and F. Ullmann. "Sources of Highly Charged Ions as a Platform Technology for Applications in Nanotechnology and Medicine" Mat.-wiss.U. Werkstofftechnik 40 (2009) 285-289.

Formatted: German (Germany)

CHAPTER 4: INTERACTION OF HIGHLY CHARGED IONS WITH SOLID SURFACES

Highly charged ions such as Kr^{27+} and Ti^{5+} carry a large amount of potential energy. As these ions approach HOPG, they interact with the HOPG. The release of the potential energy may result in novel effects occurring with the ion as well as on the surface of the substrate. The excited electronic state of the ion can decay via different tunneling processes from the substrate. In this process so-called meta-stable hollow atoms can be formed before complete decay (neutralization) of the ions happens. This transfer of electrons releases a large amount of energy in the substrate which may cause localised Coulomb explosion areas in the solid. In the near surface area of HOPG this Coulomb explosion results in substrate ions expelling each other, leading to the creation of protrusions (or hillocks) on the surface of HOPG.

This chapter is arranged as follow ion energy loss (4.1), electronic stopping power (4.1.1), nuclear stopping power (4.1.2), interaction of HCI with solids (4.2), Coulomb explosion (4.3), Coulomb explosion models (4.3.1) and formation of protrusions (4.3.2). We shall discuss the interaction of ions with solid surface in detail in this chapter.

4.1 ION ENERGY LOSS

When a charged particles pass through matter, it can ionize atoms, molecules which they encounter they collide with the stationary substrate atoms [www2]. Therefore, the charged particles lose energy in small steps. The energy loss of charged particles is described as stopping power. The stopping power relies on the energy of the charged particles and properties of the material it passes. This can be explained as the decelerating force acting on the particle during the interaction with materials. The stopping power material is numerically equivalent to the energy loss (E) per unit path length (x) written as:

$$S(E) = -\frac{dE}{dx} \tag{4.1}$$

The stopping power is divided into two independent processes, viz. electronic stopping power and nuclear stopping power. Consequently, the equation (4.1) can be written as

$$S = \left(\frac{dE}{dx}\right)_{nuclear} + \left(\frac{dE}{dx}\right)_{electronic} \tag{4.2}$$

4.1 .1 ELECTRONIC STOPPING POWER

Electronic stopping is the process where the retarding of ion projectile is caused by the inelastic collisions between bound electrons in the medium and the ion moving through it

[www2]. The process whereby energy lost is called inelastic. The excitations of bound electrons of the medium and the electron cloud of the ion are the results of collisions.

A several impact an ions encounter with electrons are high and the ion charge state travelling across the medium can alter often. All possible interactions and charge states ion are difficult to describe. The electronic stopping power can be provided as a function of energy. It is a mean taken over the energy loss processes for various charge states. It is theoretically determined to a precision of a small percentage in the energy range over several hundred keV per nucleon from theoretical treatments known as the Bethe formula. It is difficult to calculate the electronic stopping theoretically due to the energy less than 100 keV per nucleon [Sig04].

A schematic diagram of electronic stopping power and nuclear stopping power is shown in figure 4.1 below:

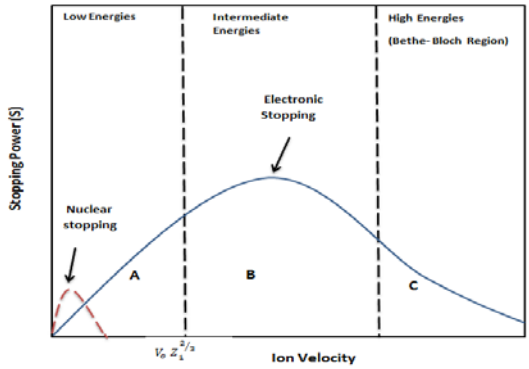

Figure 4.1: A schematic diagram of electronic stopping power and nuclear stopping power versus ion velocity. Where v_0 is the Bohr velocity [www1].

4.1 .2 NUCLEAR STOPPING POWER

Nuclear stopping power is the elastic impact between atoms in the sample and ion projectile [www2]. Nuclear stopping is not caused by the nuclear forces instead involves the ion bombardment with nuclei target. The nuclear stopping power was possible to be determined when the form of the repulsive potential energy was known in the middle of two atoms. When the mass of the ion increased, nuclear stopping also increased. At low energy, nuclear stopping was higher than the electronic stopping as shown in figure 4.1. The extremely light ions decelerate in dense material. At all energy, the nuclear stopping was weaker than the

electronic stopping. Near the surface of a solid target material, nuclear stopping can cause the sputtering.

Sputtering occurs when atoms are ejected from a target solid material cause by the interaction of the target by energetic particles. In the case of highly charged projectile ions a specific form of electronic sputtering occurs such as potential sputtering. The potential energy stored in highly charged ions is released when the ions recombine during collision on a solid surface as shown in figure 4.2.

4.2 INTERACTION OF HCI WITH SOLIDS

Modern industries have used ions interaction with surfaces in many areas including microelectronics [Bru92][Zan90][Min01]. Formerly, microelectronics only involved ions of low charge state. Here, the mechanism of the ion –surface interaction involves the KE of the ion. Due to the emergence of compact sources of HCIs with the considerably high amount of brightness, it is now possible to investigate a new regime where the internal potential energy dominates surface interaction.

The kinetic energy of ions from the HCI sources lies in the range of hundreds of keV. As such, it can be accelerated or decelerated to fit the experiment. The highest state ions in the spectrum of the naturally occurring elements can be produced by some electron beam ion sources [Schn94][Schn96][Min01]. A single ion neutralizes itself on a surface to release its potential energy. A xenon ion (Xe^{44+}) and krypton ion (Kr^{27+}) can also neutralizes themselves on a surface to release potential energy of about 51 keV and 15.5 keV respectively [www3].

In the highly charged ion regime, the ion's potential energy is more important than its kinetic energy to determine the extent of the ion–surface interaction [Sch97][Min01]. Most of the energy of single highly charged ions deposits on a solid surface in femtoseconds in a very localized area. This interaction might have practical applications [Hug95][Sch99a][Min01]. To quote from [www3], "The size of highly charged ions is relatively small compared to neutral atoms because of the reduced electronic screening of the remaining electrons in the ion". Another comparison was made by Gillaspy *et al.* [Gil01] stating that the size ratio of a hydrogen-like nickel ion to a neutral hydrogen atom is equal to the size ratio of the planet Neptune compare with the size of the Sun. Hence very small projectiles with high amount of potential energy are available for surface modifications.

In highly charged ions the highest electrostatic fields have been accomplished. For instance, the electric field of a U^{91+} ion is the range of $10^{16}\,Vcm^{-1}$ and the highly charged ion has a

huge number of unoccupied orbitals. When highly charged ions interact with a solid surface the highly charge ions trap a huge amount of electrons to the orbitals and also liberates the huge potential energy in femtoseconds onto a small region of the surface. The main purpose of highly charged ions interaction with a solid surface is a high release of secondary electron emission and terrawatts power flux deposition into a nano-region. As result this is different from that produced by the irradiation of energetic low charged ions where the kinetic energy is important.

The highly charged ions interaction with a solid surface yields huge amounts of secondary particles as result of high potential energy [www3]. The ratios of highly charged ions to secondary particles are in the range of 100 – 300 and for single charged ions is about 1. The power depositions in the range of 10^{12} – 10^{14} W/cm^2 have been released during the interaction of highly charged ion with a solid surface. This has been used to modify solid surfaces by single ion impacts. Figure 4.2 indicated the scenario of the bombardment of slow highly charged ions with solid surfaces.

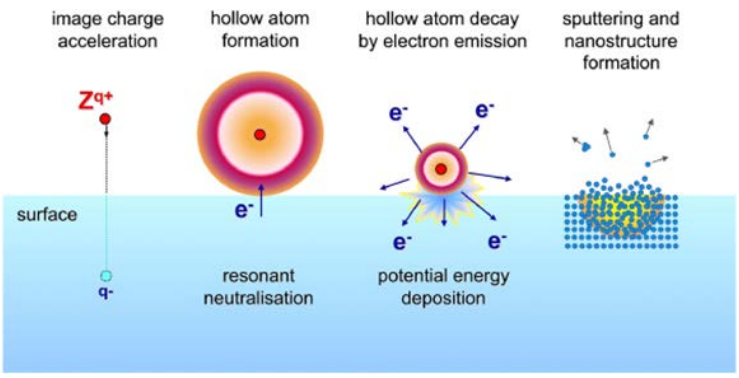

Figure 4.2: Qualitative step-by-step (in time) illustration of the processes which should take place on the approaching of a slow HCI to a rather conductive solid surface [Aum11].

As a highly charged ion interacts with a solid surface large amount of electrons are extracted from the solid surface in order to neutralize the ions. These electrons become bound in high states of the projectile to create hollow atom. The formation and decay of the hollow atom have been highly investigated [Bri90][Bur91][Arn97][Duc99][Min01].

In addition, single highly charged ions can yield large amount of disorder on a surface that can be observed by using modern scanning probe microscopy techniques.

4. 3 COULOMB EXPLOSION

Coulomb explosion is a process whereby a molecule travelling with high velocity hits a solid and then electrons that bond the molecules are ripped away quickly in collisions with the electrons of the solids; thus, the molecule is changed into a bunch of charged components that then divide under the effect of their mutual Coulomb repulsion. There are three models that describe the interaction of highly charged ions (HCI) with a solid surface. These models are described in the following subsections.

4.3.1 COULOMB EXPLOSION MODELS

Three models have been proposed to explain the response of surfaces to HCI impact. The first model states that the surface becomes locally charged because of the massive removal of electrons by the projectile [Par69][Par70][Bit79][Min01]. It has been observed that the charged volume can Coulomb explode by ejecting ions from the surface and begin a shock wave which causes the sputtering of neutral surface atoms.

The process was simulated by Cheng and Gillaspy in a molecular dynamics computation study [Chen97][Min01]. The Coulomb explosion model was initially developed for insulator targets. Parilis *et al.* [Par69] have studied that highly charged ions interacting with a solid surface can release a plasma region in nanometer scale. They have shown that the electric fields and the region explodes under mutual electrostatic repulsion occurred as a result of imbalance charge [Par70][Min01]. The Coulomb explosion model has been used to study the deposition of potential energy in solid surface caused by highly charged ions.

The plasma domain created by a slow highly charged ion bombardment is assumed to be a hemisphere with radius R, which may be obtained by the following energy balance equation [Par69][Par70]:

$$E_d = \frac{0.32\pi^2 n^2 e^2 R^5}{\varepsilon} \tag{4.3}$$

E_d is the electrostatic energy, n is the number of charge particles per volume unit, e is the electron charge and ε is the dielectric constant of the target material. Ions can accumulate kinetic energy in Coulomb explosions and can be determined by solving the equation of motion. The electrostatic energy has been deduced. The electric field distribution can be written as follows:

$$E_n^{/} = \frac{\pi ne(R-0.49r)(R-2.7h)}{R\varepsilon} \quad (4.4)$$

where E_n is the electrostatic energy of the hemisphere, R is the radius of the hemisphere, r is the distance from the centre of the hemisphere and h is the depth below the surface.

According to classical Newtonian dynamics the ions can be moved into charge region. The force is constant in a Coulomb explosion. The kinetic energy of the ion normal to the surface can be expressed as follows:

$$E_n = \frac{E_n^{/2} e^2 \tau^2}{2M} \quad (4.5)$$

Here, M and τ represent the mass of the ion and time of neutralization. The total kinetic energy of an ion that has been acquired in the Coulomb explosion process is consistent with the deposited energy. These can be calculated from the expression below:

$$E_d = \sum_i \int_v \frac{E_n^{/2} e^2 \tau^2}{2M} ndV \quad (4.6)$$

At a point where r and h are equal to zero, the maximum kinetic energy obtained by ions is expressed as:

$$E_n = E_{max} = \frac{\left(\frac{\pi neR_0}{\varepsilon}\right)^2}{2M_d} e^2\tau^2 \quad (4.7)$$

The equation above is derived from the equations (4.3) and (4.5). These can be simplified as:

$$E_{max} = \frac{1.03 E_d^{2/5} A^{1/5}}{\varepsilon_r^{3/5}} \quad (4.8)$$

where E_{max} is the maximum kinetic energy, E_d is the electrostatic energy, A is the density of charged particles and ε_r is the relative dielectric constant. Therefore, the time of neutralization of ions as they penetrate into a solid material is given by:

$$\tau = \frac{11.38 M^{1/2} \varepsilon_r^{1/2}}{A^{1/2}} \quad (4.9)$$

ε_r is the relative dielectric constant and A is the density of charged particles in the unit of $10^{22}/\text{cm}^3$. For dynamic process of the target atoms in the plasma region the following can take place such as high pressure, high temperature and period of rapid. The temperature and pressure of the multiple ions are expressed as:

$$T(\tau) = \sum_0^i \left(\frac{m_i v_i^2}{3kN}\right) = \frac{E_{k(\tau)}}{3kN} \quad (4.10)$$

and

$$p = nkT(\tau) \quad (4.11)$$

The parameters $E_k(\tau)$, N and k are the kinetic energy of ions in the plasma region at the time τ ,the number of ions in the plasma region and Boltzmann constant.

These two models allow one to get key physics estimations describing interaction of HCI with solid surface in framework of a Coulomb explosure model.

Stampfil *et al.* [Sta96] have shown that the second model used to explain the effects caused by highly charged ion bombardment on solid surfaces is similar to the structural instability model that was used to explain surface sputtering by intense laser pulses. The bombardment of highly charged ions with solid surface can yield a localized region of multiple electronic excitations. These can form covalent bonds in the lattice that can be converted to antibonding potentials and the expulsion of atoms from the surface. The mechanism was investigated by Schenkel *et al.* [Sch98] who showed that the interaction of highly charged ions with gallium arsenide can lead to high sputter yields.

The third model states that other materials, highly charged ions can liberate self-trapped excitations that can decay into colour centres causing to increase sputtering of surface particles [Var97][Min01]. This was used to explain the lithium fluoride. It can be used for a few groups of materials such as silicon dioxide and alkali halides.

Minniti *et al.* [Min01] have discussed that the interaction of slow highly charged ions with a conductive of highly oriented pyrolytic graphite (HOPG) would cause excitations and holes. They suggested that the Coulomb explosion model and the structural instability model should be investigated further.

4.3.2 FORMATION OF PROTRUSIONS

Three models have been used to explain the deposition of materials from the surface. These have been exploited as a cause of protrusions and hillocks. Terada *et al.* [Ter05] have shown the data that reveal the formation of hillocks or protrusions. The protrusions were also observed during the interaction of highly charged ions with mica. Parilis *et al.* [Par96] have explained the results of potential energy deposited on the solid surface. The three models are extensions of the Coulomb explosion model which impacts on the surface structure. Mica has a layered structure held together by ionic bonds. Due to the ions interaction on the surface layers the electrons are removed causing a net positive charge. Thus, the ionic bonds are destroyed, leading to delamination of the layers. Therefore, the Coulomb explosion model has been used to explain the interaction of highly charged ions with highly oriented pyrolytic graphite. Mica and highly oriented pyrolytic graphite are not similar [Min01]. Both have highly anisotropic layered structures, they have different bonds between the layers. In the

mica, the layers are held together by ionic bonds and highly oriented pyrolytic graphite, the layers are held together by van-der-Waals bonds. The delamination might occur in highly oriented pyrolytic graphite than in mica. Thus, the Coulomb explosion can lead to protrusion. The structural instability model can also be used, which states that a local expansion of the target can stretch the bonds from electronic excitation that can cause delamination of the layers of highly oriented pyrolytic graphite. The mechanisms can be used to determine nano-modification of the highly oriented pyrolytic graphite by highly charged ions.

The bombardment of highly charged ions with solid surface can release huge amounts of electrons from the surface due to the Coulomb explosion model. Aumayr *et al.* [Aum93] have shown, using total electron yield measurements, that a single highly charged ion with an initial charge q can remove high amount of electrons into the vacuum that is more than q. The Coulomb explosion has been quenched when the charged region was refilled with electrons before the target nuclei have been displaced. Due to the deposition from the plasma frequency the time scale of the electron motion is not more than one femtosecond. McClure *et al.* [McC64] have explained that the highly anisotropic crystal structure can lead to conductivity with huge magnitude in the plane of the surface rather than normal to the surface. This can affect the availability electrons that can neutralize the impact site.
A single highly charged ions bombardment with highly oriented pyrolytic graphite surface was not clear that the properties measured for the bulk material are important on the time and length scales. Young *et al.* [You97] have explained that the availability of two holes in a single atom of a solid can increase the time of the holes by orders of magnitude. They have assumed that the two holes are represented as a small perturbation to the lattice that cannot be used where tens or hundreds of holes are formed at the impact site. Due to silicon excited with high intensity picosecond laser pulses, it was observed by Driel *et al.* [Dri87] that the carrier diffusion decreases with increasing fluence. They have suggested that the Coulomb explosion model cannot be eliminated on the basis of bulk properties of conductivity.

The highly charged ions create the charge on the surface that has a large number of electronic excitations that can lead to a structural instability. Schenkel *et al.* [Sch99b] have shown that formerly a single highly charged ions bombardment with a silicon surface have deposited fourth percent of potential energy in electronic excitations. According to Stampfli *et al.* [Sta96] the structural instabilities can occur in graphite if seven percent of the valence electrons are excited, or at an excitation density (32 excitations/nm^3).

The potential energy of 51 keV of the Xe^{44+} ion can use the excitation density that can be deposited in excitations within a hemisphere of radius 5.4 nm. Note, in our case we consider experiments with Kr^{27+} ions which have a total stored potential energy 15 keV; it seems not enough to take this effect into account, but the situation is more precise and experimental studies are needed.

Bloembergen *et al.* [Blo93] have observed that the instability of atomic displacement begins as small as 50 femtoseconds which is faster than the time it takes for the electrons and atoms to thermalize which is about half of a picosecond. Cheng *et al.* [Chen97] have compared 50 femtoseconds with the response time during the Coulomb explosion simulations. They have studied that the highly charged ions potential energy was converted to electronic excitations with sufficient efficiency. As a result, the surface can suffer a structural instability which can cause the surface damage. Following experimental studies of HOPG surface modification by the highly charged ions, Kr^{27+} is a main goal of this work. The conditions in the experiments with Kr^{27+} are adequate for both Coulomb explosion and structural instability because both of these processes can take place in the same ion impact event.

4.4 REFERENCES

[Aum93] F. Aumayr, H. Kurz, D. Schneider, M. A. Briere, J. W. McDonald, C. E. Cunningham, and H. P. Winter. "Emission of Electrons from a Clean Gold Surface Induced by Slow, Very Highly Charged Ions at the Image Charge Acceleration Limit," Physical Review Letters 71 (1993) 1-4.

[Aum11] F. Aumayr, S. Facsko, A. S. El-Said, C. Trautmann and M. Schleberger. " Single Ion Induced Surface Nanostructures: A Comparison between Slow Highly Charged and Swift Heavy Ions" Journal of Physics: Condensed Matter 23 (2011) 393001-23.

[Arn97] A. Arnau, F. Aumayr, P. M. Echenique, M. Grether, W. Heiland, J. Limburg, R. Morgenstern et al. "Interaction of Slow Multicharged Ions With Solid Surfaces" Surface Science Reports 27 (1997) 113-239.

[Bet30] H. A. Bethe. "Theory of the transmission of corpuscular radiation through matter" Annals of Physics 5 (1930) 325-400.

[Bic63] H. Bichsel. "Handbook of Physics" section 8C (New York: McGraw-Hill) 39 (1963) 17-37.

[Bit79] I. S. Bitenskii, M. N. Murakhmetov and E. S. Parilis. "Sputtering of Non-metals by Intermediate Energy Multiply Charged Ions through a Coulomb Explosion" Soviet Physics Technical Physics 24 (1979) 618-620.

[Bor13] N. Bohr. "On the Theory of the Decrease of Velocity of Moving Electrified Particles on Passing Through Matter" The London, Edinburgh, and Dublin Philosophical Magazine and Journal of Science 25 (1913) 10-31.

[Bur91] J. Burgdörfer, P. Lerner and F. W. Meyer. "Above Surface Neutralization of Highly Charged Ions: The Classical Over the Barrier Model" Physical Review A 44 (1991) 5674-5685.

[Bri90] J. P. Briand, L. De Billy, P. Charles, and S. Essabaa Production of Hollow Atoms by the Excitation of Highly Charged Ions in Interaction with a Metallic Surface Physical Review Letters 65 (1990) 159-162.

[Bru92] C. R. Brundle,C. A. Evans, S. Wilson, and L. E. Fitzpatrick. "Encyclopedia of Materials Characterization," Butterworth-Heinemann Boston B73 (1992) 1-759.

[Blo33] F. Bloch. "To Stunt Rapidly Moving Particles during Passage Through Matter" Annals of Physics 408 (1933) 285-320.

[Blo93] N. Bloembergen. “Laser Material Interactions: Fundamentals and Applications” AIP Conference Proceedings 288 (1993) 3-12.

[Che97] H. Cheng and J. D. Gillaspy. “Nanoscale Modification of Silicon Surfaces via Coulomb Explosion” Physical Review B 55 (1997) 2628-2636.

[Duc99] J. Ducree,H. J. Andra and U. Thumm. “Neutralization of Hyperthermal Multiply Charged Ions at Surfaces: Comparison Between the Extended Dynamical Overbarrier Model and Experiment” Physical Review A 60 (1999) 3029-3043.

[Dri87] H. M. Van Driel. “Kinetics of High Density Plasmas Generated in Si by 1.06 and 0.53 μm picosecond laser pulses” Physical Review B 35 (1987) 8166-8176.

[Gil01] J. D Gillaspy. “Highly charged ions” Journal of Physics B: Atomic, Molecular and Optical Physics 34 (2001) R93-R130.

[Huo01] S. Huotari, K. Hämäläinen, C. C. Kao, R. Diamant, R. Sharon, and M. Deutsch. Resolving the Mysteries of a Hollow Atom” NSLS Activity Report 1 (2001) 2-62.

[Hug95] I. Hughes. “Charge of the Hollow Atom” Physics World 8 (1995) 43-48.

[Lin63] J. Lindhard, M. Scharff and H. E. Schiøtt. “Range Concepts and Heavy Ion Ranges (Notes on Atomic Collisions, II)” Matematisk-fysiske Meddelelser udgivet af Det ongelige Danske Videnskabernes Selskab Bind 33 (1963) 1-44.

[Mar94] R. E. Marrs, P. Beiersdorfer, and D. Schneider. “The Electron Beam Ion Trap” Physics Today 47 (1994) 27-34.

[Mar94] R. E. Marrs, S. R. Elliott and D. A. Knapp. “Production and Trapping of Hydrogenlike and Bare Uranium Ions in an Electron Beam Ion Trap” Physical Review Letters 72 (1994) 4082-4045.

[Min01] R. Minniti, L. P. Ratliff, and J. D. Gillaspy. “In-Situ Observation of Surface Modification Induced by Highly Charged Ion Bombardment” Physica Scripta T92 (2001) 22-26.

[Möl04] W. Möller. “Fundamentals of Ion Surface Interaction” Short Resume of a Lecture 1 (2004) 1-77.

[McC64] J. W. McClure. “Energy band structure of graphite” IBM Journal of Research and Development 8 (1964) 255-261.

[McD92] J. W. McDonald, D. Schneider, M. W. Clark and D. Dewitt. “Observation of High Electron Emission Yields following Highly Charged Ion Impact (up to Th^{75+}) on Surfaces” Physical Review Letters 68 (1992) 2297-2300.

[Par69] E. S. Parilis. “Sputtering, secondary emission and radiation damage” Proceedings of the International Conference on Phenomena in Ionized Gases, Bucharest 1 (1969) 94.

[Par70] E. S. Parilis. “Proceedings International Conference. Atomic Collision Phenomena in Solids” North Holland Publication Company Amsterdam (1970) 324-663.

[Par96] E. Parilis. “Radiation effects under multiply charged ion impacts” Nuclear Instruments and Methods in Physics Research Section B: Beam Interactions with Materials and Atoms 116 (1996) 478-481.

[Schm93] R. W. Schmieder and R. Bastasz. “Surface Damage caused by Single, Low Energy, High Charge State Ions” 6th International Conference on the Physics of Highly Charged Ions, American Institute of Physics 274 (1993) 690-694.

[Schn96] D. Schneider. “EBIT as a Versatile Experimental Facility” Hyperfine Interactions 99 (1996) 47-69.

[Sch97] T. Schenkel, M. A. Briere, H. Schmidt-Böcking, K. Bethge, and D. H. Schneider. “Electronic Sputtering of Thin Conductors by Neutralization of Slow Highly Charged Ions” Physical Review Letters 78 (1997) 2481-2484.

[Sch98] T. Schenkel, A. V. Hamza, A. V. Barnes, D. H. Schneider, J. C. Banks, and B. L. Doyle. “Ablation of GaAs by Intense, Ultrafast Electronic Excitation from Highly Charged Ions” Physical Review Letters 81 (1998) 2590-2593.

[Sch99a] T. Schenkel, A. V. Barnes, T. R. Niedermayr, M. Hattass, M. W. Newman, G. A. Machicoane, J. W. McDonald, A. V. Hamza, and D. H. Schneider. “Deposition of Potential Energy in Solids by Slow, Highly Charged Ions” Physical Review Letters 83 (1999) 4273-4.

[Sch99b] T. Schenkel, A. V. Hamza, A. V. Barnes, and D. H. Schneider. “Interaction of Slow, Very Highly Charged Ions With Surfaces” Progress in Surface Science 61 (1999) 23-84.

[Sig04] P. Sigmund. “Stopping of heavy ions a Theoretical Aproach” Springer Tracts in Modern Physics 204 (2004) 1-163.

[Sta96] P. Stampfli. “Electronic excitation and structural stability of solids” Nuclear Instruments and Methods in Physics Research Section B: Beam Interactions with Materials and Atoms 107 (1996) 138-145.

[Ter05] M. Terada, N. Nakamura, Y. Nakai, Y. Kanai, S. Ohtani, K. Komaki, Y. Yamazaki. “Observation of an HCI Induced Nano-dot on an HOPG Surface with STM and AFM” Nuclear Instruments and Methods in Physics Research B 235

(2005) 452-455. [Vae01]N. Vaeck, J. E. Hansen, P. Palmeri, P. Quinet, N. Zitane, M. Godefroid, S. Fritzsche, And N. Kylstra. “Hollow Atoms: A Theoretical Challenge” Physica Scripta T95 (2001) 68-75.

[Var97] P. Varga, T. Neidhart, M. Sporn, G. Libiseller, M. Schmid, F. Aumayr, and H. P. Winter.“Sputter Yields of Insulators Bombarded With Hyperthermal Multiply Charged Ions” Physica Scripta T73 (1997) 307-310.

[Wal52] M. C. Walske. “The Stopping Power of K-electrons” Physical Review 88 (1952) 1283-1289.

[Win99] H. Winter and F. Aumayr. “Hollow atoms” Journal of Physics B: Atomic, Molecular and Optical Physics 32 (1999) R39-R65.

[www1] http://www.jhaj.net/jasjeet/tcad/Learn3/13d.htm, 20th September 2013.

[www2] http://en.wikipedia.org/wiki/stopping_power(particle_radiation), 25th April 2014.

[www3] www.dreebit.com/en/ion-beam-technology/highly-charged-ions/properties-of-highly-charged-ions.html, 22nd August 2014.

[Yan08] G. Yang,W. Tieshan, L. Shengjin, H. Yuncheng, C. Liang, Y. Xiang, and X. Y. Yang. “Deposition of Potential Energy in Solid by the Interaction of Slow Highly Charged Ions with Solid Surface” 1 (2008) 1-11.

[You97] D. A Young. “On the Mechanism of the Formation of Latent Tracks in Dielectric Solids” Radiation Measurements 27 (1997) 575-586.

[Zan90] P. Van Zant. “Microchip Fabrication: a Practical Guide to Semiconductor Processing” McGraw-Hill New York 5 (1990) 97-98.

CHAPTER 5: EXPERIMENTAL PROCEDURES

Highly oriented pyrolytic graphite samples with 10 × 10 mm^2 size were irradiated with krypton and titanium ions. The nano-hillocks of the samples irradiated with ions from an electron string ion source and from an electron cyclotron resonance ion source were analysed and investigated with scanning tunneling microscopes. The experimental procedures will be discussed below.

5.1SAMPLE HOLDER DESIGN AND VACUUM CHAMBER ASSEMBLE

In order to irradiate highly oriented pyrolytic graphite samples, a new sample holder was needed. The sample holder was used in both the electron string ion source and the electron cyclotron resonance ion source. In order to obtain good results, the material from which the sample holder is created, plays an important role. The sample holder was made of brass which has a melting point in the range of 900 ^{o}C to 940 ^{o}C depending on composition. A picture of the sample holder is shown in figure 5.1. The sample holder was constructed at the University of Pretoria in the Department of Physics in South Africa. Furthermore, the vacuum chamber with precision 3D target manipulators, diagnostic systems and detectors was assembled (see figure 5.2) and tested without the ion beam of electron string ion source.

The vacuum chamber was put inside an oven at 820 ^{0}C for about 2 hours. The reason was to reduce the outgassing in order to improve the vacuum. The vacuum chamber was specifically used for the electron string ion source. The electron cyclotron resonance ion source already has a vacuum chamber. The chamber consists of a turbomolecular pump for creating high vacuum, valve gate, diaphragm, x-ray detector, manipulator, pirani gauge, cold cathode gauge and magnet.

Figure 5.1: The sample holder mounted in the electron string ion source.

The vacuum chamber was tested for leakage using helium gas and two different methods. Helium was used as a flow tracer because it penetrates small leaks very fast. It is non-toxic chemically inert and is present in the atmosphere in small quantities. In the first method, the conventional method was followed using a helium leak detector. The vacuum chamber was connected to the leak detector (see figure 5.3). The test was performed by covering the vacuum chamber with a transparent plastic bag for 3 hours. The helium was introduced into a plastic bag, thereby allowing the helium to penetrate into the vacuum chamber via leaks. The helium signal of the leak detector was continuously monitored. The total leak rate measured was in the range of 1.5×10^{-10} - 1.9×10^{-9} mbar m^3/s. In the second method, helium was introduced at high (i.e. higher than atmospheric pressure) pressure in vacuum chamber. If there is leakage from the vacuum chamber, the helium inside the vacuum chamber will pass through the leaks and the pressure will be decrease. The leak rate that measured was in the range of 2.3×10^{-11} - 2.8×10^{-10} mbar m^3/s. Although the two measured leak rates did not agree with each other, both were small enough for our experimental purposes.

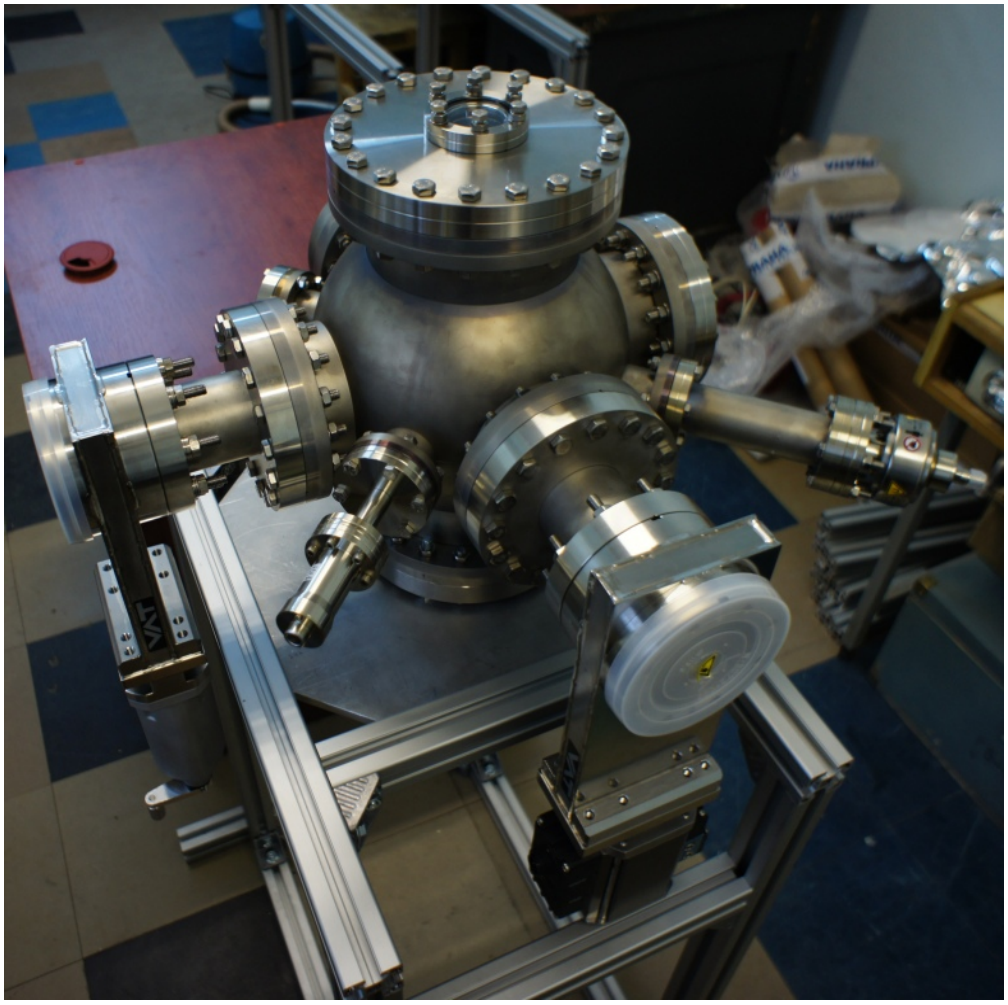

Figure 5.2: The vacuum chamber for the electron string ion source (Krion-2).

Figure 5.3: The vacuum chamber connected to the helium leak detector.

5.2 PREPARATION OF HOPG

Highly oriented pyrolytic graphite (HOPG) samples were used in this project. The samples were obtained from the Advanced Technologies Center in Moscow in Russia. Highly oriented pyrolytic graphite samples were a preferred choice for this research project due to its physical characteristics. Due to its anisotropic nature, characteristics such as electrical resistivity and thermal conductivity are not the same in directions perpendicular and along the basal plane. High oriented pyrolytic graphite remains stable at the temperatures up to five hundred degrees Celsius in air and up to two-three thousand Celsius degrees in the vacuum or inert environment.

Highly oriented pyrolytic graphite is the material created by the application of uniaxial pressure on deposited pyrocarbon at extremely high temperatures. Highly oriented pyrolytic graphite consists of an ordered stacking of basal planes and carbon atoms within the planes form hexagons. Each carbon atom is trigonally bonded to the three nearest neighbours by means of sp^2 hybridized orbitals. These hybridized orbitals result in the formation of strong covalent bonds C-C (σ). The overlap of unhybridized $2p_z$ orbitals from each carbon additionally leads to the formation of π bonds. The interaction between the basal planes is largerly dominated by the van der Waals interactions. The basal planes are stacked in the

sequence ABAB. A schematic diagram of highly oriented pyrolytic graphite is represented in chapter 1 in figure 1.1.

HOPG has a layered structure which makes it easy to be cleaved. The samples were cleaved with a 3M® Scotch Brand double sided tape in order to obtain a fresh layer of highly oriented pyrolytic graphite (HOPG) before the bombardment with ions. A piece of tape 3M® Scotch Brand double sided tape was used to pull off a thin layer of HOPG samples. The freshly cleaved sample surface was used. Before the samples were placed inside the sample holder at the end of the time-of-flight charge-to-mass spectrometer, measurements were done to find out what kind of an ion beam will bombard the samples.

5.3 IRRADIATION OF THE TARGET BY Kr^{27+} IONS FROM THE ESIS

The samples were irradiated with HCI krypton ions (i.e. Kr^{27+}) produced by the electron string ion source instrument at Joint Institute for Nuclear Research in Dubna. After the cleaning and preparation, the target was mounted to the ion collector of the time of flight mass-spectrometer. The collector was placed on the end of this device attached to a rotatable and linear movable electrical feedthrough. The facility was evacuated and internal structures of the electron string ion sources were cooled down to 77 K by liquid nitrogen and then to 4.2 K by liquid helium. The superconducting solenoid of the electron string ion source was powered and, after several tests, the ion source started to provide the Kr^{27+} beam. The beams of highly charged ions Kr^{27+} were extracted from an electron extractor with a kinetic energy of about 0 to 100 eV× q (q = 27). The kinetic energy spread of the extracted Kr^{27+} ions bombarding the target was in the range of 0 - 2.7 keV. The potential energy of Kr^{27+} ions during the experiment was 15.54 keV, which means that the maximum kinetic energy of the ions of 2.7 keV was only 17 percent of its potential energy. Initially the target was not placed inside the sample holder and the beam condition was measured by the ion current on the collector. When it was seen that the ion beam was proper, then the sample was placed inside the sample holder. The collector was turned for the sample to be irradiated.

The signal from the collector was amplified by the preamplifier, shown by the oscilloscope and stored for further analyses. The number of highly charged ions on the target in each pulse was equal to 2×10^6 ions of Kr^{27+} per pulse. The electron string ion source produced ion pulses with a frequency of one pulse in each four seconds and total irradiated time was 140 minutes that provided 2100 pulses. The total number Kr^{27+} ions impacting on the HOPG target of 10 x 10 mm^2 was 4.2×10^9 Kr^{27+} ions on the target of 10 x 10 mm^2 or, equivalently,

42 Kr^{27+} ions per micron^2. After the irradiation the facility was stopped and the target was removed from the setup for further STM scanning.

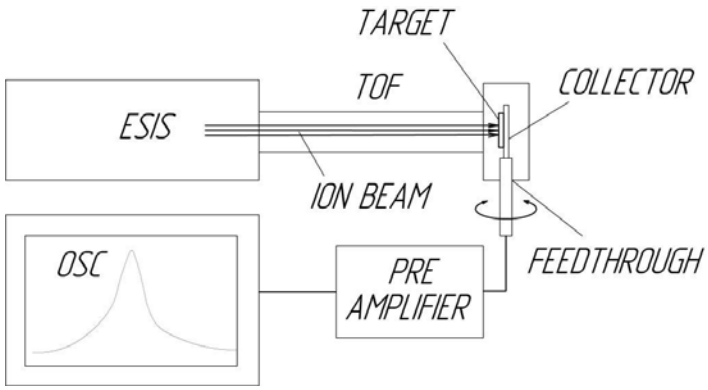

Figure 5.4: A schematic diagram of the setup for irradiation of the target by the ions produced in the ESIS.

5.4 IRRADIATION OF THE TARGET BY Ti^{5+} IONS FROM THE ECR

The samples were irradiated with titanium ions (viz. Ti^{5+}) by electron cyclotron resonance ion source instrument at Joint Institute for Nuclear Research in Dubna. In figure 5.5 the end section of the beam line is presented. Before loading of the target, the target box was disconnected from the test and diagnostic box. Then the target box connected to the diagnostic box was evacuated and the HOPG target was irradiated. The condition and the composition of the ion beam were measured by the diagnostic box. The kinetic energy of the ions was 50 keV. The number of highly charged ions on the target in each pulse was equal to 1.1 x 10^9 ions of Ti^{5+} per pulse. The total irradiated time was about 10 minutes that provided 150 pulses. Therefore, the total of irradiated Ti^{5+} ion beams on the HOPG target of 10 x 10 mm^2 was 1.6 x 10^{11} ions. This means that the samples were irradiated with Ti^{5+} ion beam up to a total fluence 1.6 x 10^{11} cm^{-2}. After the irradiation the gate valve was closed and the sample was unloaded for STM scanning.

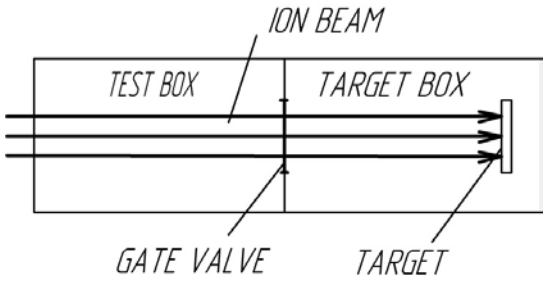

Figure 5.5: A schematic diagram of the setup for irradiation of the target by the ions produced in the ECR.

5.5 STM MEASURENTS

The surface topographies of the samples were investigated with a scanning tunnelling microscopy (STM) at Moscow University in Russia and at University of Pretoria in South Africa. An STM can operate in either constant height mode or in the constant tunnelling current mode as mentioned in chapter 3. In this research project, all measurements were performed in the constant tunnelling current mode. The HOPG sample was placed on the sample holder using tweezers. The Pt/Ir tips (Model PT10) of 0.25 mm in diameter were used, which was good for STM since they do not scratch the HOPG samples. The tip did not crash on the sample throughout the experiment due to good settings in the software and the electrical connections. The bias between the AFM head and the sample was tested and it corresponded with the settings in the software. The measured noise level was 0.1 nm prior to the experimental measurements.

The bias voltage used to the HOPG sample allows the tunnelling current to flow. The bias voltage was used 10 to 1000 mV and the tunnelling current was used 10 nA. The feedback gains were put high, the tunnelling probe tips nearly tracked the HOPG surface and the variations in the height needed to maintain constant tunnelling current was measured by the change in the voltage used to the piezoelectric tube. The following different scan sizes were used ; for HOPG samples irradiated with Kr^{27+} ions, viz. 350 x 950 nm^2, 400 x 600 nm^2, 500 x 500 nm^2 and 2000 x 2000 nm^2 respectively; and for HOPG samples irradiated with Ti^{5+} ions they were 500 x 650 nm^2 and 700 x 700 nm^2 respectively.

CHAPTER 6: RESULTS AND DISCUSSION

This chapter 6 discusses the results of this study. An electron string ion source (krion-2) and electron cyclotron resonance ion source were used to bombard highly oriented pyrolytic graphite samples with multiple highly charged ions of Kr^{27+} and Ti^{5+}. A scanning tunnelling microscope was utilised to investigate the changes occurring on the highly oriented pyrolytic graphite (HOPG) samples after bombardment with ion beams. The highly oriented pyrolytic graphite (HOPG) samples were kept in a clean container to avoid contamination. Before irradiation, a piece of tape was used to cleave the highly oriented pyrolytic graphite layers, in order to leave a fresh (virgin) graphite surface. Electron string ion source (krion-2) and electron cyclotron resonance ion source were used for the different reasons as discussed previously in chapter 3.

For Kr^{27+} with the use of the Krion-2 electron string ion source: Highly oriented pyrolytic graphite (HOPG) samples were irradiated by the beam of krypton ions of a mean charge state Kr^{27+} (plus few neighbouring charge states). Kr^{27+} ions have a total potential energy $E^{Kr27+}{}_{pot}$ = 15.54 keV (which is the sum of the binding energies of all 27 removed electrons). As it was described in chapter 2 (section 2.2.5), these Kr^{27+} ions also had a kinetic energy in a range $E^{Kr27+}{}_{kin}$ = 0 - 2.7 keV. Thus the influence of the potential energy of Kr^{27+} ions on irradiated HOPG is dominant in this experiment, since $E^{Kr27+}{}_{kin} \leq 0.17\, E^{Kr27+}{}_{pot}$. The total fluence of a Kr^{27+} ion beam was about 4.2×10^9 cm^{-2} Kr^{27+} on the HOPG target.

As will be seen in the results presented below, the dimensions of the artifacts created by the highly charged ions on the surfaces of HOPG are very small and thus difficult to distinguish from contamination. Consequently, a key factor in identifying them in STM images is to correlate the density of the artifacts with the density of ion impacts as calculated from the ion fluence.

The measurement (measuring the total ion charge on the target; target - HOPG sample $10 \times 10 = 100$ mm^2) of Kr^{27+} ion beam on the target was about 2×10^6 ions of Kr^{27+} per pulse. Krion-2 ESIS produced ion pulses with a working frequency of 1 pulse every 4 seconds. Total irradiation time was 140 minutes, which means a total of 140 x 60 / 4 = 2100 pulses. Hence the total number Kr^{27+} ions impacting on the HOPG target of 10 x 10 mm^2 was $2x10^6 \times 2100 = 4.2 \times 10^9$ Kr^{27+} ions on the target of 10 x 10 mm^2 or equivalently,

42 Kr^{27+} ions per micron^2 (1 micron = 10^{-3} mm, so total HOPG target area is 10^8 μ^2). The value of 42 Kr^{27+} ions per micron^2 is an averaged value since the ions could be distributed non-uniformly in space. Thus, we expect that in a central part of ion beam this density can be in the range of 10 – 100 ions per micron^2. To summarize: total density of Kr^{27+} ions on the HOPG target could vary from 42 Kr^{27+} ions per μm^2 to 4200 Kr^{27+} ions per μm^2.

For Ti^{5+} with the use of the electron cyclotron resonance ion source: Highly oriented pyrolytic graphite (HOPG) samples of the same size (10 x 10 mm^2) were irradiated by Ti^{5+} ions to a fluence of 1.6 x 10^{11} cm^{-2} Ti^{5+} on a HOPG target. The potential energy of a Ti^{5+} ion is $E^{Ti5+}{}_{pot}$ = 0.185 keV, and its kinetic energy $E^{Ti5+}{}_{kin}$ = 50 keV. Thus, in this experiment with a Ti^{5+} ion beam, the effect of ion kinetic energy is strongly dominant since $E^{Ti5+}{}_{kin} \approx 270\ E^{Ti5+}{}_{pot}$.

6.1 SCANNING TUNNELLING MICROSCOPE (STM) RESULTS WITH Kr^{27+} IONS

The surface damage (or modifications) of highly oriented pyrolytic graphite after irradiated with Kr^{27+} and Ti^{5+} ions was investigated using the scanning tunnelling microscope in NanoScan Company, Moscow State University. The constant tunnelling current mode was used to analyse the highly oriented pyrolytic graphite samples. Figures 6.1 below show the topography of the highly oriented pyrolytic graphite samples surfaces after the Kr^{27+} bombardment. Due to the potential energy of highly charged ions, this can lead to a modification of the highly oriented pyrolytic graphite samples. The potential energy deposited on the solid surface would expand, causing the destruction of the lattice structure. A disordered structure can be produced on the surface as shown in figure 6.1. The instrument and image parameters, such as the tunnelling current, scan speed, image contrast, etc., were varied to obtain the best resolution in the images. This was done in order to observe the topographical effect on flat surface of the sample due to individual ion bombardment. In figure 6.1(a) (i.e. the lowest magnification image with a scan size of 2000 x 2000 nm^2) the lamella structure of HOPG is visible at the right of the image. The planes of covalent-bonded carbon atoms are not perfectly flat. At this level of magnification, the topographical effect of the bombarding ions is not visible. At the next level magnification (i.e. scan size of 500 x 500 nm^2), shown in figure 6.1(b), the same observations, as per figure 6.1(a) can be made. Figure 6.1(c) contains too much noise to make any meaningful conclusions from.

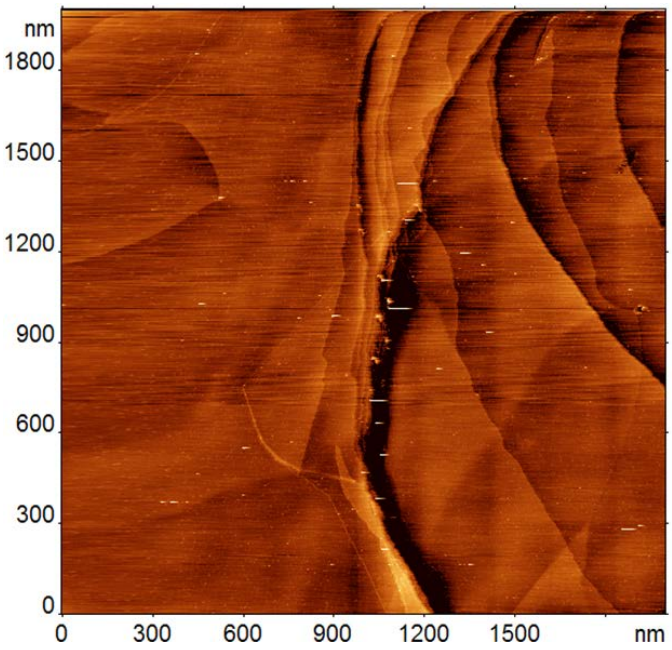

(a)

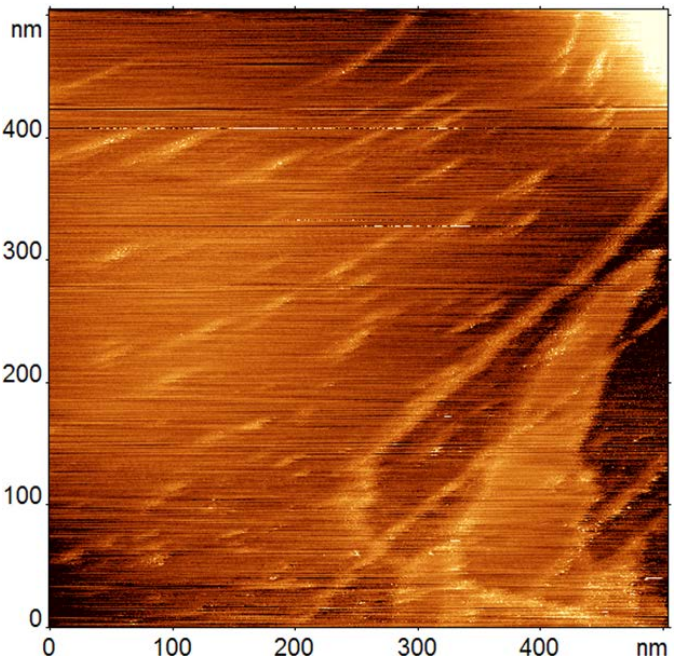

(b)

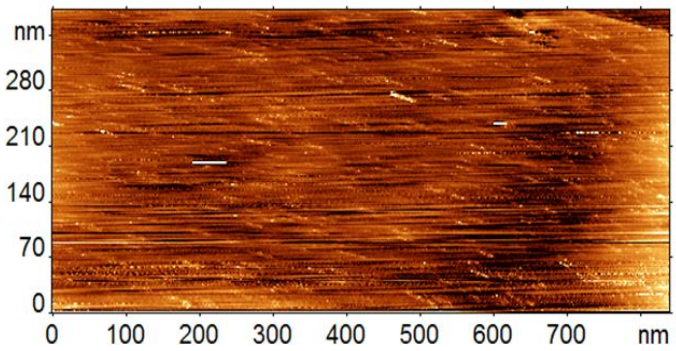

(c)

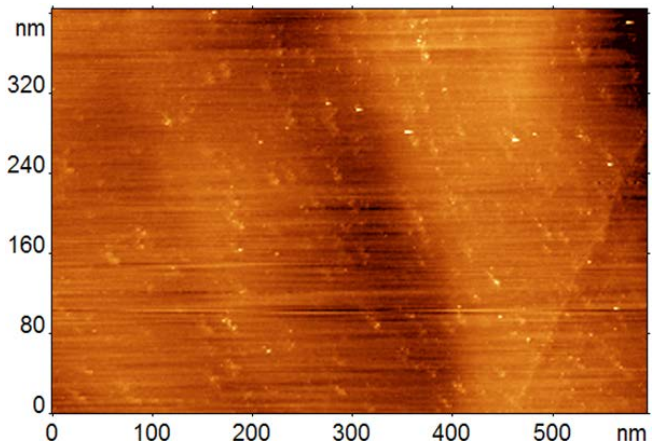

(d)

Figure 6.1: Different scan sized STM images of HOPG samples irradiated with Kr^{27+}ions (a) 2000 x 2000 nm (b) 500 x 500 nm (c) 350 x 950 nm (d) 400 x 600 nm sizes.

Figure 6.1 (d) is of a particular interest since it has the highest spatial resolution among all images (Figure 6.1 a-d). “White dots”, visible on this image are nano-modifications, caused by the Kr^{27+} ions impact. A “control” non-irradiated HOPG sample has been scanned with the same spatial resolution by the same STM just one hour after scanning the irradiated samples. There were no white dots observed on the image of this unbombarded HOPG sample. The visible concentration of “white dots” in the figure 6.1 (d) (total number of the dots is about 50 on the area 400 x 600 nm x nm = 0.24 μm^2) gives an approximate concentration of 200 dots/μm^2, which is in agreement with the fluence estimation given above: 42 - 4200 μm^{-2}. Thus, with a high probability of certainty, one can consider these “white dots” originating as a result of the Kr^{27+} ions impacting on a HOPG surface.

From the STM measurements, one can make two important observations:

- The visible structural changes of the HOPG surface allow us to consider them as protrusions (or hillocks) rather than craters (holes).
- The approximate lateral size of the protrusions is 5 - 7 nm.

Note, the observed structural changes are due to the potential energy interaction of the Kr^{27+} ions with the HOPG substrate, rather than their kinetic energy interaction, which would create holes due to sputtering [Aum11].

6.2 SCANNING TUNNELLING MICROSCOPE (STM) RESULTS WITH Ti^{5+} IONS

"White dots" were observed in the STM images of the HOPG surface irradiated by the Ti^{5+} ions beam with an incident kinetic energy 50 keV, see figure 6.2 (a-b) below. The constant tunnelling current mode was used to analyse the HOPG samples. However, the estimated dot concentration in these images is about 90 dots / μm^2 which were much less than was estimated with beam fluence 1.6×10^{11} cm^{-2} giving a concentration of 1.6×10^3 dots μm^{-2}.
This disagreement could perhaps be explained by beam defocusing on target; but this explanation is not satisfactory. Thus, in contrast to the previous case with irradiation with Kr^{27+} ions, we are less sure about identification of these white dots with swift Ti^{5+} ion impacts. We can estimate lateral size of the possible nano-dots as 10 - 12 nm. This value definitely contradicts the expected value (2 - 4 nm) for Ti^{5+} ions and is in contradiction with the results of other groups; see table 6.1 below. Thus, the observed white dots on figure 6.2(a) and figure 6.2(b) are rather artefacts (probably contamination) than real HOPG modifications caused by ion impact.

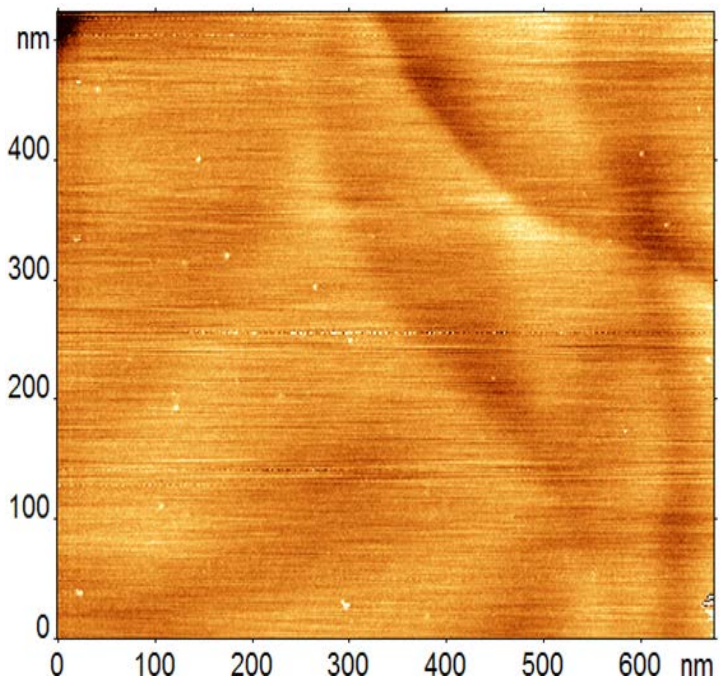

(a)

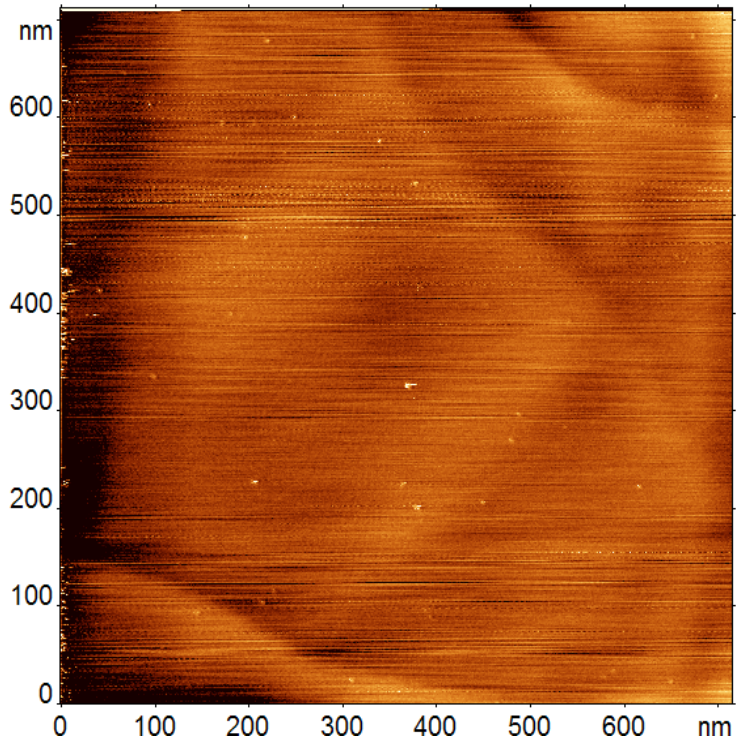

(b)

Figure 6.2: STM image of HOPG samples irradiated with Ti^{5+} ions (a) 500 x 650 nm (b) 700 x 700 nm sizes.

6.3 DISCUSSION OF THE RESULTS

It would be interesting to compare our STM results with those obtained by other groups. However, the different groups used different (to our) highly charged ions (HCI) with various charge states (and hence potential energy of highly charged ions) and different incident ion kinetic energies. The average protrusion sizes of their STM results and our results are presented in table 6.1.

Table 6.1: Summary of average protrusion size (dot) induced by highly charged ions impact on HOPG.

ION SPECIES	POTENTIAL ENERGY (keV)	KINETIC ENERGY (keV)	DOT DIAMETER (nm)	DOT HEIGHT	DOT HEIGHT	REFERENCE
Xe^{46+}	66	138	6	0.5	0.5	[Ter05]
Xe^{44+}	51	276	7	0.8	-	[Min01]
Kr^{27+}	15.5	2.7	5-7	-	-	This study
Xe^{23+}	6.8	276	3	0.5	-	[Min01]
Ar^{9+}	1.0	0.15	1.2	0.3	-	[Geb03]
Ar^{8+}	0.6	4	1.2	0.5	-	[Moc97]
Ar^{8+}	0.6	0.4	1.0	-	-	[Meg01]
Ti^{5+}	0.185	50	10	-	-	This study

In table 6.1 the results are tabled in decreasing order of the potential energies of the ions. From this it can be seen that the average diameter of the nano-dots on the HOPG also decreases in correspondence with the decrease in potential energy. This correlation of HCI induced topography with the potential energy was already discussed and explained in section 4.3.

There are two sets of results, which exhibit small discrepancies with this trend. They are the Ar^{8+} results by Mochiji *et al.* [Moc97] and Meguro *et al.* [Meg01] and the results for the Xe^{46+} ions of Terada *et al.* [Ter05] and for the Xe^{44+} ions of Minniti *et al.* [Min01]. In the latter, the average dot diameter size for Xe^{46+} ions was 6 nm while for the Xe^{44+} ions, with less potential energy, the average dot size was 7 nm. The fact that two sizes are so near to

each other, and that were measured by different groups using different instruments mean the difference between the dot diameter sizes are probably within the experimental errors of both sets of measurements. A similar conclusion can be made with the other set exhibiting a small discrepancy. Since both Mochiji *et al.* [Moc97] and Meguro *et al.* used Ar^{8+} ions, the potential energy of the ions was the same in both cases with the only difference being the kinetic energy. Although the dot sizes of 1.2 nm and 1.0 nm reflected the difference in kinetic energy, it is unlikely that the kinetic energies could be the explanation for the dot size differences. These two sizes are again so near to each other that the experimental error in the measurements by the different groups is probably the more likely explanation.

There is only significant exception to our statement that there is a correlation between the average protrusion diameter and the potential energy of the ions. This exception is the average dot size on HOPG by our Ti^{5+} ions. The average diameter is much larger than what follows from the trend in table 6.1. As was discussed in section 6.2, these dots were probably contamination spots. The fact that the number of these protrusions was significantly less than the number of ions impinging on the surface of the samples further confirms this conclusion.

The average diameter of our protrusions on HOPG created by Kr^{27+} ions is clearly within the trend of the decrease of average dot diameter size with decreasing ion potential energy. Consequently, we are comfortable with our identification of the white dots in our STM images, shown and discussed in section 6.1, as being protrusions caused on the HOPG by the bombarding Kr^{27+} ions.

Further analysis has to be done for the spatial image resolution of our samples (figure 6.1, figure 6.2) to study in greater detail the observed protrusions. In order to get a spatial image resolution of 10 x 10 nm^2, one needs to focus the cantilever of the STM exactly on the protrusions. One needs to take many images with a low scan rate to obtain some protrusion. Independent analysis of the irradiated samples was planned in Pretoria, in order to confirm (or contradict) the obtained results. Moreover, it was planned to use a highest possible resolution in order to study details of protrusions. Unfortunately, the results of such studies with Nanoscope scanning tunnelling microscope (Pretoria, South Africa) were negative. The reason for this failure was incorrect sample preparation before scanning, which led to the fatal destruction of the HOPG surface modified by HCI bombardment.

The main benefit of the work involved in this study is a successful collaboration between the two groups in Dubna, Russia and the University of Pretoria, South Africa. Furthermore, it led

to an appraisal of the methodology for irradiation of the sample surfaces by highly charged ions and the analysis of these samples. Further studies are planned for the near future.

6.4 REFERENCES

[Aum08] F. Aumayr, A. S. El-Said, and W. Meissl. “Nano-sized Surface Modifications Induced by the Impact of Slow Highly Charged Ions a First Review” Nuclear Instruments and Methods in Physics Research Section B: Beam Interactions with Materials and Atoms 266 (2008) 2729-2735.

[Aum11] F. Aumayr, S. Facsko, A. S. El-Said, C. Trautmann, and M. Schleberger. “Single Ion Induced Surface Nanostructures: A Comparison between Slow Highly Charged and Swift Heavy Ions” Journal of Physics: Condensed Matter 23 (2011) 393001-23.

[Bur06] J. Burgdörfer, C. Lemell, K. Schiessl, B. Solleder, C. Reinhold, and L. Wirtz. “Collisions of Slow Highly Charged Ions with Surfaces’’ arXiv preprint Physics 0605245 (2006) 1-13.

[Geb03] I. Gebeshuber, S. Cernusca, F. Aumayr, H. Winter. “Nanoscopic Surface Modification by Slow Ion Bombardment” International Journal of Mass Spectrum 229 (2003) 27-34.

[Liu11] S. Liu, M. Sakurai, W. Zhang, K. Asakura, N. Iida, M. Tona, T. Terui, T. Sakurai, and H. Ohta. “SEM and ESR Measurements on HOPG Surfaces Irradiated With Ar^{11+} and Ar^{1+}” Physica Scripta T144 (2011) 014043-5.

[Lop05] I. Lopez-Salido, D. C. Lim, and Y. D. Kim. “Ag Nanoparticles on Highly Ordered Pyrolytic Graphite (HOPG) Surfaces Studied using STM and XPS” Surface Science 588 (2005) 6-18.

[Meg01] T. Meguro, A. Hida, M. Suzuki, Y. Koguchi, H. Takai, Y. Yamamoto, K. Maeda, Y. Aoyagi. “Creation of Nano-diamonds by Single Impacts of Highly Charged Ions Upon Graphite” Applied Physics Letters 23 (2001) 3866-3868.

[Min01] R. Minniti, L. P. Ratliff, and J. D. Gillaspy. “In-Situ Observation of Surface Modification Induced by Highly Charged Ion Bombardment” Physica Scripta T92 (2001) 22-26.

[Moc97] K. Mochiji, S. Yamamoto, H. Shimizu, S. Ohtani, T. Seguchi, N. Kobayashi. “Scanning Tunneling Microscopy and Atomic Force Microscopy Study of Graphite Defects Produced by Bombarding with Highly Charged Ions” Journal of Applied Physics 82 (1997) 6037-6040.

[McC92] R. L. McCarley, S. A. Hendricks and A. J. Bard. “Controlled Nanofabrication of Highly Oriented Pyrolytic Graphite with the Scanning Tunneling Microscope” The Journal of Physical Chemistry 96 (1992) 10089-10092.

[Ton04] M. Tona, and S. Takahashi. “Highly Charged Ion Beams From the Tokyo EBIT For Applications to Nano-Science and Technology” In Journal of Physics: Conference Series. IOP Publishing 2 (2004) 57-64.

[Ter05] M. Terada, N. Nakamura, Y. Nakai, Y. Kanai, S. Ohtani, K. Komati, Y. Yamazaki. “Observation of an HCI induced nano-dot on an HOPG surface with STM and AFM” Nuclear Instruments and Methods in Physics Research B 235 (2005) 452-455.

[Wac13] G. Wachter, K. Tőkési, G. Betz, C. Lemell, and J. Burgdörfer. “Modelling Surface Restructuring by Slow Highly Charged Ions” Nuclear Instruments and Methods in Physics Research Section B: Beam Interactions with Materials and Atoms 317 (2013) 149-153.

CHAPTER 7: SUMMARY

A number of different kinds of ion sources that produced singly charged or multi-charged ions have been developed since in 1834. The ion sources differ in their methods of producing ions. The singly charged or multi-charged ions can be created due to electron impact ionization of atoms or molecules in ion sources. Multi-charged ions can be produced by different ion sources as mentioned in this research. There are many types of ions sources which are capable of producing ions with low charge state. The production of highly charged ions with a charged state greater than ten is possible with electron beam ion source (EBIS), its modification electron string ion source (ESIS), and electron cyclotron resonance ion source (ECR). The production of highly charged ions (HCI) by these three ion sources were discussed in detail in chapter 2. In this project we have used electron cyclotron resonance ion sources and electron string ion sources to produce the multi-charged ion beams. The multi-charged ion beams can be used in different fields. The two instruments were used to irradiate highly oriented pyrolytic graphite samples at Veksler and Baldin Laboratory of High Energies (VBLHE, JINR, Dubna) with the Krion-2 electron string ion source and electron cyclotron resonance ion sources at the Flerov Laboratory of Nuclear Reactions (FLNR, JINR, Dubna) irradiation facility.

The basic principles and equations for the production HCI were reviewed together the design and operating principles of the electron string ion source and electron cyclotron resonance ion source. In a review of ion-solid interactions, special attention was given to the interaction of HCI with solid surfaces and the possible mechanisms operating during this type of interaction.

We have designed the sample holder for electron string ion source and electron cyclotron resonance ion source. The sample holder was manufactured at the University of Pretoria in the Department of Physics in South Africa. For this study I also assisted in the assembling of the vacuum chamber in Dubna, Russia and tested whether it had any vacuum leaks. The vacuum chamber was specifically constructed for the electron string ion source. An electron cyclotron resonance ion source has a vacuum chamber.

In this study the surface modifications on highly oriented pyrolytic graphite after irradiated with Kr^{27+} and Ti^{5+} ions were investigated using the scanning tunnelling microscope in NanoScan Company, Moscow State University. On both sets of samples small white dots, i.e.

protrusions, were observed on the HOPG samples after irradiation. The average sizes of these dots were determined and compared to those of other studies using different HCI ions with different potential energies and kinetic energies. This comparison showed that there is a correlation between the average protrusion diameter and the potential energy of the HCI. This finding is line with previous investigations and agrees with the theory of HCI interactions with solids as extensively discussed in the above mentioned review.

In this study the potential energy of our Ti^{5+} ions was 0.185 keV (which is the sum of the binding energies of all 5 removed electrons) and its kinetic energy was 50 keV. Thus, in this experiment the effect of ion kinetic energy is strongly dominant since $E^{Ti5+}{}_{kin} \approx 270\, E^{Ti5+}{}_{pot}$. STM scans of the HOPG surfaces after ion bombardment showed small protrusions on the surfaces. The average areal concentration (i.e. number of protrusions per area) of these nano-dots was much less than the ion fluence (i.e. number of ions per area) received by the samples. Furthermore, the average dot diameter was much more than the average HCI bombardment-induced protrusion diameter found in other studies and also our Kr^{27+} investigation. Consequently, we identified these dots as being contamination spots.

Our Kr^{27+} ions had a potential energy 15.54 keV, while the kinetic energy ranged from 0 to 2.7 keV. This means that the maximum kinetic energy of the ions was only 17 percent of its potential energy. The average protrusion diameter of our bombardment-induced protrusions on HOPG as measured by STM was 5 to 7 nm. This average protrusion diameter as a function of the potential energy of the ions was compared to the results of other studies. Our results fitted well within the correlation of average protrusion diameter and the potential energy of the HCI. Furthermore, the average areal concentration (i.e. number of protrusions per area) of the nano-dots agreed with the ion fluence received by the samples. This is a further proof of identifying the dots observed on the HOPG as being caused by the ion bombardment.

7.1 POSSIBLE FUTURE INVESTIGATIONS

Investigation of the high charge regime that will reveal a mechanism of ion-surface interactions that rely on the potential energy rather than its kinetic energy should follow. The theoretical models which were described in this research were used to explain the interaction of highly charged ions with solid surface. New experiments with various kinds of highly charged ions and with different samples are needed.

These experiments can also be done with the use of new Krion-6T ESIS (VBLHE, JINR, Dubna) which can produce intense ion beams of highly charged ions of heavy elements, like Au^{69+}. A non-destructive sample analysis methodology coupled with the use of modern scanning tunneling microscope or atomic force microscope in non-contact mode of operation should be further investigated as well.